Polymer Chemistry

Accepted Manuscript

This article can be cited before page numbers have been issued, to do this please use: A. C. S. Gonzalez, R. T. Aroso, C. Cunha, J. S. Seixas de Melo, M. E. S. Eusébio, T. Maria, G. J. da Silva, P. F. Cruz, R. M. M. Brito, R. M. B. Carrilho and M. M. Pereira, *Polym. Chem.*, 2026, DOI: 10.1039/D5PY01211B.

View Article Online
DOI: 10.1039/D5PY01211B

ARTICLE

CO_2-derived functional polycarbonates as a sustainable platform for photosensitive polymeric materials

Received 00th January 20xx,
Accepted 00th January 20xx

DOI: 10.1039/x0xx00000x

Andreia C. S. Gonzalez,[a] Rafael T. Aroso,[a] Carla Cunha,[a] J. Sérgio Seixas de Melo,[a] M. Ermelinda S. Eusébio,[a] Teresa M. R. Maria,[a] Gabriela J. da Silva,[b] Pedro F. Cruz,[a] Rui M. M. Brito,[a] Rui M. B. Carrilho*[a] and Mariette M. Pereira *[a]

The development of CO_2-based polymers integrating photo-responsiveness, synthetic versatility and processability remains an important challenge in polymer chemistry. Herein, a modular strategy was developed for multifunctional CO_2-derived photosensitive polycarbonates. Catalytic copolymerisation of CO_2 and 1,2-epoxy-4-vinylcyclohexene using tetrapyrrolic macrocyclic metal complexes (Cr porphyrin or Al phthalocyanine) as dual-function catalysts and embedded photosensitisers afforded polycarbonates with high carbonate incorporation (95-99%) and preserved photophysical features. Pendant vinyl groups enabled post-polymerisation modification, through an unprecedented Rh-catalysed hydroformylation introducing formyl groups with remarkable chemo- and regioselectivity, while bromination with Br_2 provided an additional functionalisation route. Comprehensive structural, spectroscopic and thermal characterisation confirmed the robustness and tunability of the materials. Notably, the Al-phthalocyanine-based polycarbonates retained key photophysical properties of the photosensitiser (ϕ_F up to 0.46, ϕ_Δ up to 0.21). To overcome polymer brittleness, an ethyl cellulose-based biocomposite film incorporating the formyl-functionalised polycarbonate was prepared, leading to improved flexibility and thermal stability. The formyl-functionalised polymer and the corresponding biocomposite film exhibited strong photo-antibacterial activity, completely eradicating *Staphylococcus aureus* (≥7-log CFU reduction) under red light (660 nm, 49 J·cm^{-2}), highlighting the potential of CO_2-derived photosensitive polycarbonates for light-responsive environmental applications.

Introduction

Photosensitive polymers are a class of compounds that undergo specific chemical or physical transformations upon exposure to light, ranging from UV to visible or near-infrared (NIR) wavelengths, enabling their integration into diverse applications such as semiconductors, optical data storage, biomedical devices and smart functional coatings.[1-5] Typical photoactive groups, such as azobenzenes[6] (reversible *trans–cis* isomerisation), coumarins[7] and cinnamates[8] (photodimerisation or cleavage), or spiropyrans[9] (light-induced structural rearrangements), can be incorporated directly into the polymer backbone or as pendant side chains. Photosensitive polymers are particularly relevant in photodynamic therapy (PDT) and antimicrobial photodynamic inactivation (*a*PDI), where they may work both as carriers and photosensitisers.[10-16] For instance, porphyrin-loaded polymeric nanoparticles have been shown to achieve effective tumour regression,[17] while cationic conjugated polymers demonstrated high phototoxicity against multidrug-resistant bacteria under visible light, through strong membrane binding and efficient ROS generation.[18] Photosensitive polymers also show great potential in photocatalysis and optoelectronics, enabling visible-light harvesting for solar-driven environmental remediation and hydrogen generation.[19] Among photosensitive polymers, polycarbonates are particularly attractive due to their combination of mechanical strength, optical transparency and thermal stability, supporting advanced applications in microelectronics, sensors, microfluidic devices, drug delivery and smart packaging.[20-23] Light-responsive polycarbonates are typically prepared by embedding photoactive groups during step-growth polymerisation of bisphenol-based monomers with carbonyl sources (*e.g.*, phosgene, diphenyl carbonate),[24,25] or by ring-opening polymerisation (ROP) of cyclic carbonates carrying photosensitive substituents, allowing precise functional group distribution in high-molecular-weight polymers.[26,27] Post-polymerisation modifications further expand their design possibilities by grafting photoactive moieties onto reactive sites (e.g. hydroxyl terminal groups), thereby fine-tuning photophysical behaviour without compromising polymer integrity.[28,29] Despite these advances, the large-scale synthesis of photosensitive polycarbonates remains constrained by the toxicity and sustainability issues of conventional reagents, such as phosgene or acyl chlorides. Alternatively, the production of CO_2-derived polycarbonates through catalytic copolymerisation of CO_2 and epoxides offers a

[a] Coimbra Chemistry Centre, Institute of Molecular Sciences (CQC-IMS), Department of Chemistry, University of Coimbra, 3004-535 Coimbra, Portugal
E-mails: rui.carrilho@uc.pt; mmpereira@qui.uc.pt
[b] Faculdade de Farmácia e Centro de Neurociências e Biologia Celular, University of Coimbra, Pólo das Ciências da Saúde, Azinhaga de Santa Comba, 3000-548 Coimbra, Portugal

Electronic Supplementary Information (ESI) available: [Characterization of all polymers (NMR, SEC, X-ray diffraction, FTIR)]. See DOI: 10.1039/x0xx00000x

versatile and greener route for polycarbonate synthesis, reducing the environmental impact.[30-34] When applied to 1,2-epoxy-4-vinylcyclohexene, this approach generates vinyl-functionalised polycarbonates that are highly amenable to post-polymer modification.[35-50] However, although this functionalisation strategy has been explored for a range of chemical transformations and applications, its potential for the development of multifunctional photosensitive polycarbonates remains, to the best of our knowledge, still unexplored. In addition, polycarbonates typically form materials that are intrinsically rigid and brittle.[51] In this context, blending polycarbonates with bio-based cellulose derivatives as plasticisers represents a promising strategy to enhance their mechanical performance and expand their practical applicability.[52,53]

In this study, we report a sustainable one-step synthesis of CO_2-based photosensitive polycarbonates, in which tetrapyrrolic metal complexes (aluminium phthalocyanine or chromium porphyrin) act simultaneously as CO_2/epoxide copolymerisation catalysts and embedded photosensitisers (Fig. 1). Post-polymer functionalisation of vinyl groups *via* unprecedented Rh-catalysed hydroformylation and bromination enable the tuning of their physical and thermal properties, as demonstrated by comprehensive structural, spectroscopic and thermal characterisations. The photosensitive behaviour of the polymers originates from the embedded tetrapyrrolic macrocycles, while post-polymerisation functionalisation was intended to tune the thermal and mechanical properties of the resulting materials. To overcome the intrinsic brittleness of neat polycarbonates, we further developed a polycarbonate/ethyl cellulose biocomposite film with enhanced flexibility while preserving the relevant photophysical features. In addition, all materials were preliminarily investigated in antimicrobial photodynamic inactivation (*a*PDI) studies to assess their potential for the development of light-triggered disinfectant surfaces or coatings.

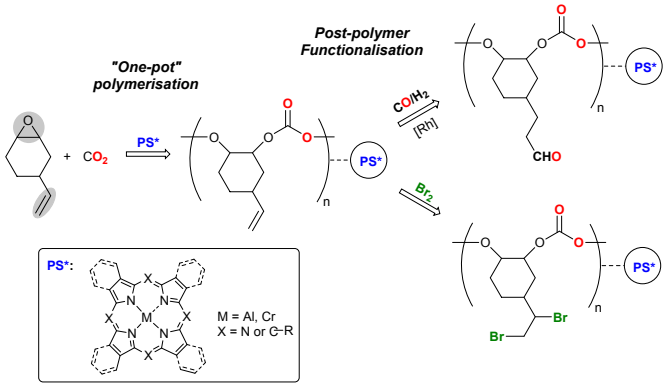

Fig. 1 Envisioned synthetic strategy for CO_2-derived photosensitive polycarbonates.

Results and discussion

Synthesis of CO_2-derived photosensitive polycarbonates

The strategy for developing CO_2-derived photosensitive polymers, with tunable structures and light absorption properties, began with the synthesis of poly(4-vinylcyclohexene)carbonate through catalytic copolymerisation between 1,2-epoxy-4-vinylcyclohexene and carbon dioxide

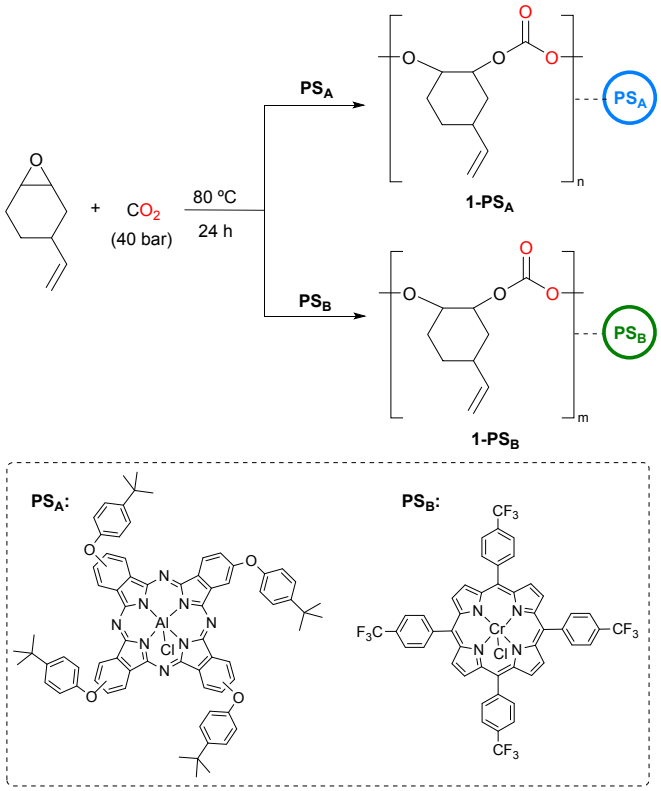

(Scheme 1).

Scheme 1 Synthesis of photosensitive polycarbonates **1-PS$_A$** and **1-PS$_B$** *via* CO_2/epoxide catalytic copolymerization, using Al-phthalocyanine (**PS$_A$**) or Cr-porphyrin (**PS$_B$**) as catalysts and photosensitizers.

We employed two catalysts previously developed by our group,[33,34] both of which have demonstrated high catalytic activity and selectivity for polycarbonate formation: tetrakis(4-tert-butylphenoxy)phthalocyaninatoaluminium(III) chloride (**PS$_A$**) and tetrakis(4-trifluoromethylphenyl)porphyrinatochromium(III) chloride (**PS$_B$**). We envisaged that **PS$_A$** and **PS$_B$** would fulfil a dual function, acting both as Lewis acid catalysts for polymerisation and as embedded chromophores, enabling the straightforward preparation of photosensitive polycarbonate materials. The polymerisation conditions were previously optimised, using **PS$_B$** catalyst, through systematic evaluation of the effects of temperature (50-80 °C) and CO_2 pressure (10-50 bar) on the catalytic activity, polymer selectivity and CO_2 incorporation. Reactions conducted at 50 °C resulted in conversions below 80%, whereas increasing the temperature to 80 °C led to significantly higher conversions (ca. 90%), indicating improved catalytic efficiency at this temperature. Regarding CO_2 pressure, 40 bar was identified as optimal, since at 10 bar CO_2, lower conversion was observed (ca. 70%), while increasing the pressure to 50 bar did not provide further improvement compared to 40 bar. Moreover, these variations in temperature

View Article Online
DOI: 10.1039/D5PY01211B

and CO_2 pressure did not produce significant differences in polymer selectivity or in the degree of CO_2 incorporation.

Accordingly, using the optimised conditions, the tetrapyrrolic macrocycle catalyst and the cocatalyst, bis(triphenylphosphine)iminium chloride (PPNCl), were mixed with the epoxide substrate inside a glass-lined stainless-steel autoclave. The vessel was then pressurised with CO_2 (40 bar), and the reaction was conducted at 80 °C for 24 h. After completion, the crude was analysed by ^{1}H NMR to determine the conversion. The remaining epoxide was evaporated and the selectivity for polymer formation was calculated. Finally, the solid residue was washed with *n*-hexane and dried to remove the cyclic carbonate trace contents, and the CO_2 content in the polycarbonate material was determined. These results are presented in Table 1.

Table 1 Catalytic copolymerization between CO_2 and 1,2-epoxy-4-vinylcyclohexene, using Al(III) phthalocyanine (**PS$_A$**) and Cr(III) porphyrin (**PS$_B$**) catalysts

Cat.	Conv.(%)[a]	TON/TOF(h^{-1})[b]	Select. (%)[c]	CO_2 content (%)[d]	Yield (%)
PS$_A$	55	786/33	75	95	38
PS$_B$	90	1286/54	94	99	80

Reaction conditions: epoxide (31 mmol, 4 mL), catalyst: 0.07 mol %, cocatalyst: PPNCl 0.07 mol %, T = 80 °C, P_{CO_2} = 40 bar; t = 24 h; [a] % Conversion determined by ^{1}H NMR; [b] turnover number calculated as mol(converted substrate)/mol(catalyst); turnover frequency calculated as turnover number / hour; [c] selectivity for polymers determined by ^{1}H NMR; [d] % CO_2 incorporation determined by ^{1}H NMR, through integral ratio of carbonate linkage peak/(carbonate + ether linkages peaks).

The Al(III) phthalocyanine catalyst (**PS$_A$**) achieved 55% conversion after 24 h (TON = 786, TOF = 33 h^{-1}), exhibiting good catalytic performance with 75% selectivity toward polymer formation (25% identified as cyclic carbonate product). In comparison, the Cr(III) porphyrin catalyst (**PS$_B$**) demonstrated superior catalytic performance under identical conditions, achieving 90% conversion (TON = 1286, TOF = 54 h^{-1}) and a markedly higher polymer selectivity of 94%. Notably, both catalysts yielded copolymers with high levels of CO_2 incorporation (95-99%), composed predominantly of carbonate linkages and containing only minor proportions of ether linkages, approximately 5% in **1-PS$_A$** and 1% in **1-PS$_B$**, as determined by ^{1}H NMR (Fig. S1 and Fig. S7, SI). The high levels of CO_2 incorporation observed are comparable to some of the highest values previously reported for vinyl cyclohexene polycarbonates,[36,39-50] and exceed other achieved with double metal cyanides (DMCs)[35] and nickel phenolate catalysts.[37,38]

The differences in catalytic performance between **PS$_A$** and **PS$_B$** can be attributed to their distinct electronic and structural characteristics. The chromium porphyrin **PS$_B$**, bearing strongly electron-withdrawing trifluoromethyl substituents, increases the Lewis acidity of the metal centre, thereby promoting epoxide activation and facilitating CO_2 insertion, which accounts for its higher catalytic activity. In contrast, the aluminium phthalocyanine **PS$_A$** possesses a more electron-rich macrocyclic environment and is more prone to intermolecular aggregation due to its extended planar aromatic structure, which may reduce the effective Lewis acidity of the metal centre, resulting in comparatively lower catalytic activity.

MALDI-TOF MS analysis, recorded in positive ion mode using DIT as matrix and NaTFA as cationization agent (Figs. S23–S24, SI), revealed a distribution of oligomeric species detected mainly as sodium adducts $[M+Na]^+$, in which M represents the neutral oligomeric chain. For **1-PS$_A$**, signals in the range ca. 1050-1600 m/z can be assigned to oligomeric species containing approximately 5-8 carbonate repeating units. For example, peaks at m/z 1036.8, 1205.2, 1373.9 and 1547.6 are consistent with sodium adducts of oligomers bearing chloride-containing end groups, in agreement with initiation by Cl^-. In addition, peaks at m/z 1125.4 and 1294.3 are consistent with oligomers incorporating one ether linkage, as supported by NMR analysis, and bearing hydroxyl-containing end groups. The spectrum also exhibits a second group of peaks at higher masses (ca. 2160-2350 m/z), which indicates the presence of polymer-photosensitiser-associated ions (e.g., $[M+PS_A+Na]^+$). In contrast, the MALDI-TOF spectrum of **1-PS$_B$** displays a well-defined oligomeric distribution with a regular peak spacing of 168 Da, consistent with the expected -$C_8H_{12}OC(O)O$- fragment, corresponding to the 4-vinylcyclohexylcarbonate repeating unit formed. Peaks observed at m/z 1005.5, 1173.5, 1341.6, 1509.7, 1677.7 and 1846.8 correspond to oligomeric Na adducts containing n = 5-10 repeating units, respectively, bearing two terminal -OH groups. Additional peaks located at approximately 1023.4, 1527.6 and 1864.8 m/z are consistent with oligomers bearing one -OH and one -Cl terminal groups.[33] The absence of polymer-photosensitiser-associated ions in the case of **1-PS$_B$**, together with the contrasting behaviour observed for **1-PS$_A$**, suggests that the structure of the photosensitiser may influence the ionisation behaviour. Overall, the MALDI-TOF data are consistent with initiation by Cl^- together with chain transfer and/or hydrolysis processes, in agreement with the established coordination-insertion mechanism for epoxide/CO_2 copolymerization using metalloporphyrin/PPNCl catalytic systems.[33-34]

The resulting polymeric materials, **1-PS$_A$** and **1-PS$_B$**, preserved both the characteristic colour and the absorption profiles of the parent catalysts/photosensitizers, **PS$_A$** and **PS$_B$**. Specifically, **1-PS$_A$** exhibited a blue colour with λ_{ax} = 680-685 nm, while **1-PS$_B$** displayed a green colour with λ_{ax} = 437-445 nm (Fig. 2). These results indicate that the photophysical properties of the polymers arise from the tetrapyrrolic macrocycles, which remain embedded and electronically intact within the polymer matrix.

To further investigate the possible linkage between the photosensitizer and the polymer chains, ^{1}H NMR DOSY experiments were performed. Polymer **1-PS$_B$** was shown to exhibit a significantly lower diffusion coefficient than **1-PS$_A$**, indicating longer polymer chains (Fig. S9, SI), consistent with GPC/SEC data (Table 2). In both samples, the low photosensitizer content (0.4-3%) prevented reliable diffusion

View Article Online
DOI: 10.1039/D5PM01211F

correlations between the aromatic signals of the photosensitizer (δ ≈ 6.5-8.5 ppm) and the polymer backbone signals (δ ≈ 0.5-6.0 ppm). Therefore, an additional ^{1}H NMR DOSY experiment, performed after adding more **PS$_A$** to **1-PS$_A$** samples showed identical diffusion coefficients for the aromatic signals of **PS$_A$** and the polymer backbone (Fig. S10, SI), indicating close association and suggesting that the photosensitizer is physically embedded within the polymer matrix through non-covalent interactions (e.g., van der Waals interactions). A similar DOSY NMR analysis for **1-PS$_B$**, was not feasible due to the paramagnetic nature of the chromium (III) porphyrin, which limits the acquisition of reliable diffusion data.

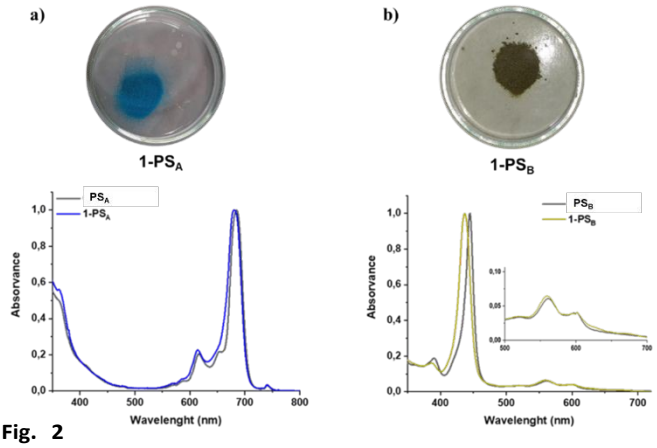

Fig. 2 Images of photosensitive polycarbonate powders: a) **1-PS$_A$**; b) **1-PS$_B$**, and their normalized UV-Vis spectra, using 2-Me-THF as solvent.

To access functionalised photosensitive polycarbonates, taking advantage of the pendant vinyl groups present in the polymer backbone, we proceeded with the Rh-catalysed hydroformylation of vinyl-functionalised polycarbonates **1-PS$_A$** and **1-PS$_B$**, using 9,9-dimethyl-9H-xanthene-4,5-diyl)bis(diphenylphosphane (xantphos) as phosphorus ligand, in order to maximise the selectivity for linear aldehydes formation.[54-56] The vinyl polymer **1-PS$_A$** or **1-PS$_B$**, along with the rhodium precursor $Rh(CO)_2(acac)$ and xantphos, were placed into a glass-lined stainless-steel autoclave. Toluene was then added, the system was pressurised to 20 bar with an equimolar mixture of CO/H_2 and the mixture was stirred at 80 °C for 5 h (Scheme 2, *via* A). The solvent was then removed under reduced pressure, and the resulting solid was washed with *n*-hexane and dried under vacuum.

The hydroformylation of vinyl polycarbonate **1-PS$_A$** proceeded with complete conversion into the corresponding formyl-functionalised polycarbonate **2-PS$_A$**. This transformation was confirmed by ^{1}H NMR spectroscopy, through disappearance of the signals at 5.05 and 5.76 ppm, assigned to the vinylic protons, and the presence of a single signal at 9.78 ppm, characteristic of aldehyde protons resonance, showing full chemoselectivity towards aldehydes and the exclusive formation of polycarbonate chains bearing linear aldehyde groups (Fig. S3, SI). Consequently, the target photosensitive polycarbonate **2-PS$_A$**, incorporating aluminium phthalocyanine photosensitisers, was successfully isolated as a light blue powder in 88% yield. Under identical reaction conditions, the hydroformylation of vinyl polycarbonate **1-PS$_B$** resulted in the formation of a green solid, which exhibited complete insolubility in a wide range of solvents, including *n*-hexane, toluene, dichloromethane, acetone, ethyl acetate, DMF, DMSO, methanol and water. The insolubility of formyl-functionalised polycarbonate **2-PS$_B$** suggests the possible formation of a higher molecular-weight cross-linked polymer network. After washing with *n*-hexane and dichloromethane, the photosensitive polycarbonate **2-PS$_B$** was isolated in 92% yield.

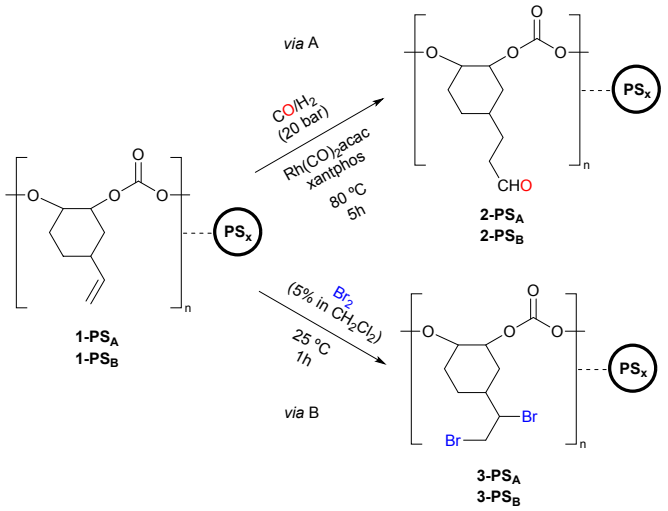

Scheme 2 Post-polymer functionalisation of photosensitive polycarbonates **1-PS$_A$** and **1-PS$_B$** through Rh-catalysed hydroformylation (*via* A) and bromination (*via* B).

A different approach towards multifunctional photosensitive polycarbonates was carried out, through bromination of the pendant vinyl groups (Scheme 2, *via* B). In a typical procedure, vinyl polycarbonates **1-PS$_A$** or **1-PS$_B$** were reacted with a 5% solution of Br_2 in CH_2Cl_2. Bromination of **1-PS$_A$** and **1-PS$_B$** proceeded with complete conversion after 1 h, as confirmed by ^{1}H NMR spectra of the crude mixtures, showing no signals of characteristic vinyl protons. Upon work-up, the resulting solids were washed with brine and dried under vacuum, to afford the brominated polycarbonates **3-PS$_A$** and **3-PS$_B$**, as bluish green powders with isolated yields of 90% and 86%, respectively.

The amount of photosensitiser incorporated into the polymer matrices was quantified by ICP-MS, through determination of the Al or Cr metal contents. For **PS$_A$**-based polymers (**1-PS$_A$**, **2-PS$_A$**, **3-PS$_A$**), the Al-phthalocyanine contents were 3.0%, 2.8%, and 1.7%, respectively, while for **PS$_B$**-based polymers (**1-PS$_B$**, **2-PS$_B$**, **3-PS$_B$**) the Cr-porphyrin levels were 0.41%, 0.28%, and 0.24%. The higher relative amount of **PS$_A$** compared with **PS$_B$** reflects the lower polymerisation conversion and isolated yield obtained with the Al catalyst, resulting in the same amount of catalyst (0.07 mol %) being distributed over a smaller mass of polymer obtained.

The photosensitive polycarbonates were characterised by size exclusion chromatography (GPC/SEC). Measurements were performed in tetrahydrofuran, against polystyrene standards,

View Article Online
DOI: 10.1039/D5PY01211B

enabling determination of the number-average (M_n) and weight-average (M_w) molecular weights and dispersity ($Đ = M_w/M_n$). The results are summarised in Table 2.

The GPC chromatograms of vinyl polycarbonates **1-PS$_A$** and **1-PS$_B$**, obtained *via* CO_2/epoxide copolymerisation, both display a unimodal elution profile, indicative of polymers with relatively uniform chain lengths and low dispersity. However, the presence of a slight shoulder on the elution curves points to minor fractions of lower molecular weight species (Figs. S11 and S14, SI). In contrast, the modified polycarbonates **2-PS$_A$**, **3-PS$_A$** and **3-PS$_B$** showed bimodal or polymodal elution profiles, characterised by broader peaks or multiple distinct peaks (Figs. S12, S13 and S15, SI).

Table 2 GPC/SEC data of photosensitive polycarbonates

Entry	Polymer	$M_n \times 10^3$ ($gmol^{-1}$)	$M_w \times 10^3$ ($gmol^{-1}$)	Đ (M_w/M_n)	$M_{n,th} \times 10^3$ ($gmol^{-1}$)
1	**1-PS$_A$**	2.9	3.6	1.24	97.8[a]
2	**1-PS$_B$**	11.2	15.8	1.41	202.5[a]
3	**2-PS$_A$**	4.5	13.0	2.88	3.4[b]
4	**2-PS$_B$**	n.d.*	n.d.*	n.d.*	-
5	**3-PS$_A$**	1.3	2.1	1.62	5.7[b]
6	**3-PS$_B$**	10.5	14.7	1.40	21.9

Analysis were performed against a polystyrene standard, using THF as solvent. M_n: number-average molecular weight; M_w: weight-average molecular weight; $Đ=M_w/M_n$: dispersity.

* Not determined due to insolubility of **2-PS$_B$**.

[a] $M_{n,theory}$ calculated from monomer-to-cocatalyst ratio, epoxide conversion, selectivity and carbonate incorporation.

[b] $M_{n,theory}$ calculated from M_n of vinyl polymer precursor and repeat-unit mass increase, assuming quantitative functionalization and no chain scission/coupling.

These features suggest that hydroformylation and bromination, as post-polymer modifications, lead to the formation of polymer mixtures comprising chains with varying lengths and molecular weights. The vinyl cyclohexene polycarbonate **1-PS$_A$**, prepared via CO_2/epoxide copolymerisation with aluminium phthalocyanine catalyst (**PS$_A$**), exhibits low number and weight average molecular weights (M_w = 3.6 × 10^3 $gmol^{-1}$; M_n = 2.9 × 10^3 $gmol^{-1}$), consistent with oligomers formation. In contrast, chromium porphyrin catalyst (**PS$_B$**) yields **1-PS$_B$** with significantly higher molecular weight (M_w = 15.8 × 10^3 $gmol^{-1}$ and M_n = 11.2 × 10^3 $gmol^{-1}$), clearly demonstrating the effect of the tetrapyrrolic metal catalyst on the polymerisation process (Table 2, entries 1-2). These differences may reflect variations in propagation efficiency and in the relative rates of chain-transfer or termination processes for each catalytic system. The greater electrophilicity of the chromium centre likely favours more efficient chain growth, whereas the aluminium-based system might experience more chain-transfer events, resulting in shorter polymer chains.

The M_n values obtained by SEC/GPC are significantly lower than the theoretical values estimated from the monomer-to-cocatalyst ratio, assuming one growing chain per equivalent of PPNCl. This discrepancy can be rationalised by the apparent molecular weights derived from polystyrene calibration, together with the likely presence of multiple initiating species, leading to a higher number of polymer chains and consequently lower experimental M_n values. The dispersity (M_w/M_n) values of 1.2 (for **1-PS$_A$**) and 1.41 (for **1-PS$_B$**) indicate that the polymer chains exhibit relatively uniform lengths and molecular weights, reflecting narrow and well-controlled molecular weight distributions. These values represent a significant improvement over the broader distributions for 4-vinylcyclohexane polycarbonate, obtained with other catalysts, previously reported in the literature.[35] GPC analysis further revealed that hydroformylation of polycarbonate **1-PS$_A$** yielded a structurally distinct polycarbonate **2-PS$_A$**, accompanied by a notable increase in M_w from 3.6 × 10^3 $gmol^{-1}$ to 13.0 × 10^3 $gmol^{-1}$ and a substantial rise in M_n from 2.9 × 10^3 $gmol^{-1}$ to 4.5 × 10^3 $gmol^{-1}$, indicating the formation of polymer chains with significantly higher molecular weights (Table 2, entries 1 and 3). This increase points toward the occurrence of intermolecular crosslinking between formyl-functionalised polymer chains, through aldol-type reactions (Scheme S1, SI). These findings are consistent with the ^{1}H NMR analysis of **2-PS$_A$**, which shows a lower-than-expected integration value for the aldehyde proton signal at 9.78 ppm (Fig. S3, SI). This phenomenon also results in a significantly higher dispersity for **2-PS$_A$** (Đ = 2.88), indicating a broad molecular weight distribution compared to the more uniform profiles typically observed for the vinyl-based polycarbonates **1-PS$_A$**. For **2-PSA**, $M_{n,theory}$ was calculated from M_n of vinyl polymer precursor (**1-PS$_A$**) and the repeat-unit mass increase expected upon quantitative hydroformylation. The higher M_n determined by SEC/GPC relative to this theoretical value indicates partial intermolecular coupling during modification, consistent with the ^{1}H NMR data. In the case of the brominated polycarbonates **3-PS$_A$** and **3-PS$_B$**, a decrease in both number-average (M_n) and weight-average (M_w) molecular weights was observed relative to their vinyl-functionalised precursors (Table 2, entries 5 and 6). This diminution may be attributed to chain cleavage processes occurring during bromination, potentially triggered by side reactions or partial degradation of the polymer backbone.[57] Consistently, $M_{n,theory}$ values calculated assuming quantitative dibromination and no chain scission, predict a substantially higher molecular weight. The lower values experimentally observed therefore strongly supports the occurrence of chain cleavage processes during bromination.

Fourier-transform infrared (FTIR) spectra of the photosensitive polycarbonates (Fig. 3) consistently show two absorption bands in the 2937-2855 cm^{-1} region, assigned to aliphatic C–H stretching vibrations, together with intense carbonyl (C=O) stretching bands at 1735-1738 cm^{-1}, characteristic of carbonate functionalities.[58] Additionally, intense bands near 1235 cm^{-1} are attributed to C–O stretching vibrations within the carbonate moiety. The presence of these vibrational modes confirms the preservation of the polycarbonate backbone across all samples. For the vinyl-functionalised polycarbonates **1-PS$_A$** and **1-PS$_B$**, weak absorption bands at 3074 cm^{-1} and 1640 cm^{-1} are detected, corresponding to the C–H and C=C stretching vibrations of olefinic groups. Additionally, comparison between the FTIR spectra of **1-PS$_A$** and **1-PS$_B$** reveals an additional

absorption band at 1080 cm^{-1} in **1-PS$_B$**, characteristic of C–O stretching in ether bonds, which suggest the presence of minor ether linkages when aluminium phthalocyanine is used as the copolymerisation catalyst (Table 1, entry 1), corroborating the ^{1}H NMR data (Fig. S1, SI). The FTIR spectra of polymers **2-PS$_A$** and **2-PS$_B$** retain the carbonate carbonyl stretching band, which overlaps with the C=O stretching of the introduced formyl groups. Deconvolution of the carbonyl region reveals two distinct bands at 1818 cm^{-1} and 1721 cm^{-1}, attributed to carbonate and aldehyde carbonyls, respectively (Fig. S22, SI). The disappearance of the alkene C–H stretching band at 3074 cm^{-1}, coupled with the appearance of a new band at 2725 cm^{-1}, characteristic of aldehyde C–H stretching, provides further evidence of successful hydroformylation. Regarding the brominated polycarbonates **3-PS$_A$** and **3-PS$_B$**, the FTIR spectra exhibit complete disappearance of the alkene-related bands at 3074 and 1640 cm^{-1}, consistent with the absence of the vinyl groups.[59]

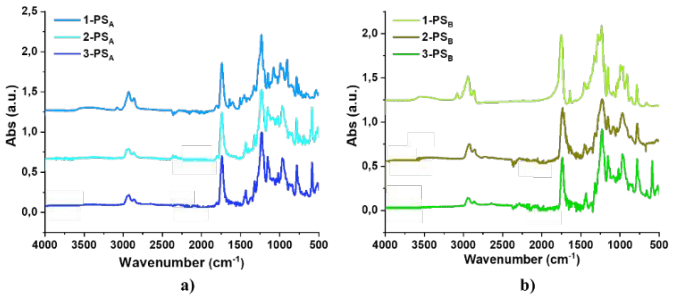

Fig. 3 FTIR spectra of photosensitive polycarbonates: a) **1-PS$_A$**, **2-PS$_A$** and **3-PS$_A$**; b) **1-PS$_B$**, **2-PS$_B$** and **3-PS$_B$**.

To gain insight into the morphological features of the photosensitive polycarbonates, high-resolution surface images were acquired by scanning electron microscopy (SEM), shown in Fig. 4.

As observed, all samples displayed non-uniform particles, forming dense agglomerates of faceted and irregular shapes, with fragmented surfaces and a broad size distribution enriched in submicron aggregates. This pronounced fragmentation seen in all samples suggests limited plastic deformation, a characteristic typical of alkyl polycarbonates.[60,61] Comparative analysis of vinyl polycarbonates **1-PS$_A$** and **1-PS$_B$** revealed that the higher molecular weight polymer **1-PS$_B$**, obtained with the chromium porphyrin catalyst **PS$_B$**, formed larger particles than **1-PS$_A$**, highlighting a catalyst-dependent effect on polymer growth and microstructure. Furthermore, formyl-functionalised polycarbonates **2-PS$_A$** and **2-PS$_B$** displayed distinctly different morphologies, characterised by uniform lamellar particles with smooth surfaces and sharp edges, generally larger than their vinyl analogues. In contrast, brominated polycarbonates **3-PS$_A$** and **3-PS$_B$** exhibited intermediate particle sizes and morphologies, consistent with a balance between amorphous and semi-ordered domains imparted by bromine addition.

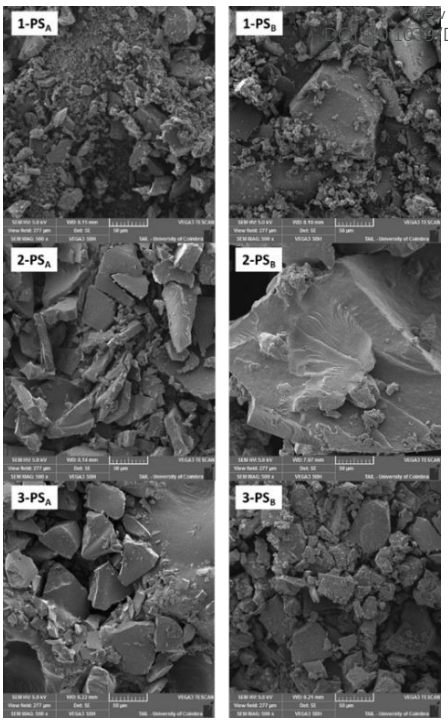

Fig. 4 SEM images of photosensitive polycarbonates (with 500× magnification).

Thermal stability of polycarbonates

The thermal stability of the photosensitive polycarbonates was systematically investigated through thermogravimetric analysis (TGA) and differential scanning calorimetry (DSC). The TGA/DTG curves (Fig. 5) reveal different degradation profiles according to the chemical modifications introduced into the initial vinyl polycarbonate **1-PS$_A$** or **1-PS$_B$**. Post-polymer functionalisation via hydroformylation or bromination markedly influence their degradation mechanism and thermal stability, as reflected by variations in the maximum degradation temperature (T_{max}) and the temperatures corresponding to 5% and 50% mass loss (T_5 and T_{50}, respectively), as shown in Table 3.

Table 3 Thermal degradation temperatures of photosensitive polycarbonates **1–3-PS$_A$** and **1–3-PS$_B$**

Polymer	T_5/°C	T_{50}/°C	T_{max}/°C
1-PS$_A$	168	223	207
2-PS$_A$	164	282	200
3-PS$_A$	190	237	242
1-PS$_B$	177	203	206
2-PS$_B$	250	309	297
3-PS$_B$	188	261	266

T_5 = temperature at 5% weight loss, T_{50} = temperature at 50% weight loss, T_{max} = temperature at maximum degradation rate.

Distinct thermal degradation profiles were obtained for each **PS$_A$** and **PS$_B$** series, corresponding to the degree and type of chemical functionalisation. The initial decomposition temperatures, T_5, which indicate the temperature of measurable weight loss, provide an early indication of the

thermal robustness of the materials. For the vinyl-functionalised polycarbonate **1-PS$_A$**, a T_5 of 168 °C suggests the presence of thermally labile end groups or low molecular weight fractions, consistent with its low molecular weight. This is followed by a main decomposition event at T_{max} = 207 °C and a broader weight loss culminating at T_{50} = 223 °C, with a secondary degradation peak at 412 °C likely associated with residual backbone degradation. For the formyl polymer **2-PS$_A$**, a similar T_5 of 164 °C was observed, implying that initial labile sites remain, but T_{50} markedly increased to 282 °C, and additional degradation steps at 286 °C and 417 °C indicate more complex thermal breakdown pathways, possibly involving oxidation of aldehyde functionalities.

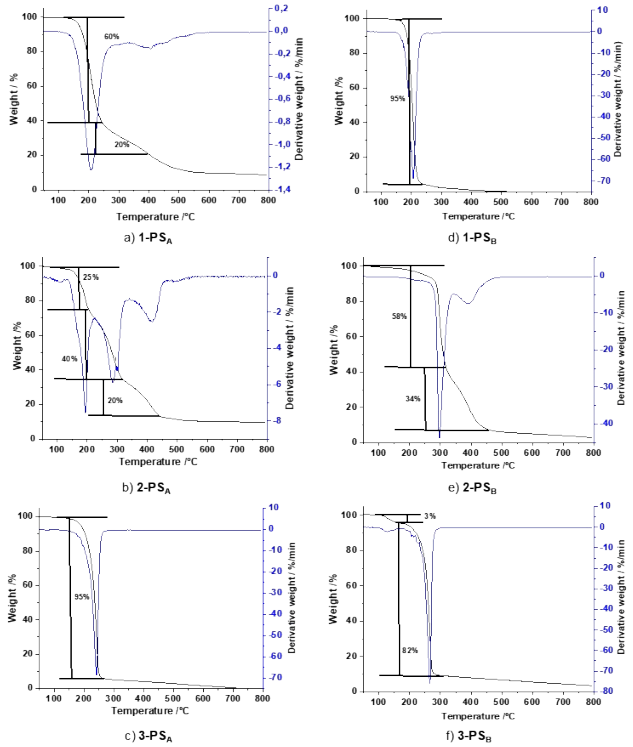

Fig. 5 TGA/DTG plots of photosensitive polycarbonates **1–3-PS$_A$** and **1–3-PS$_B$**.

The brominated derivative **3-PS$_A$** shows a higher T_5 of 190 °C, with T_{max} = 242 °C and T_{50} = 237 °C, reflecting an overall increase in thermal resistance, likely due to steric hindrance and the stabilizing influence of the bromine atoms.[62] Regarding the **PS$_B$** series, the vinyl-functionalised polycarbonate **1-PS$_B$** presents T_5 = 177 °C, slightly higher than that of its analogue **1-PS$_A$**, suggesting marginally improved initial stability due to the longer polymer chains. The subsequent relatively narrow degradation window (T_{max} = 206 °C and T_{50} = 203 °C) is indicative of a uniform degradation process. In contrast, the formyl-functionalised polymer **2-PS$_B$** exhibits a pronounced increase in thermal resistance, with T_5 = 250 °C, T_{max} = 297 °C and T_{50} = 309 °C. The corresponding DTG curve shows an additional maximum at 390 °C, consistent with a more thermally stable network structure, potentially arising from higher intermolecular interactions or partial crosslinking induced by the formyl groups.[63] The brominated polycarbonate **3-PS$_B$** (with T_5 = 188 °C, T_{max} = 266 °C, T_{50} = 261 °C) also demonstrated improved stability over **1-PS$_B$**, associated with steric hindrance and restricted chain mobility, though to a lesser extent than **2-PS$_B$**, likely due to the occurrence of chain cleavage.[64]

Complementary differential scanning calorimetry (DSC) measurements were then performed to investigate the precise determination of glass transition temperatures, offering deeper insight into the segmental mobility and chain rigidity of the polymers (Fig. 6). The vinyl-functionalised polycarbonate **1-PS$_A$** exhibits a T_g at ~50 °C, characteristic of flexible aliphatic chains with pendant vinyl groups. Upon hydroformylation, T_g increases to 89 °C in **2-PS$_A$**, which reflects increased rigidity and restricted mobility due to the polar aldehyde groups that may enhance interchain interactions.[63] In contrast, the T_g of **3-PS$_A$** remains at ~50 °C, suggesting that bromination, while increasing thermal stability, does not significantly affect chain mobility. Regarding the **PS$_B$** series, the vinyl polycarbonate **1-PS$_B$** shows a T_g at ~87 °C, which aligns with expectations for reduced segmental motion in longer chains. The formyl-functionalised polycarbonate **2-PS$_B$** displays two distinct T_g values at 65 °C and 105 °C, indicating phase heterogeneity, possibly due to partial crosslinking or microphase separation between modified and unmodified domains. On the other hand, the brominated polycarbonate **3-PS$_B$** presents a T_g of ~77 °C, slightly lower than that of **1-PS$_B$**, attributed to increased flexibility, possibly due to chain cleavage upon bromination.[57,64]

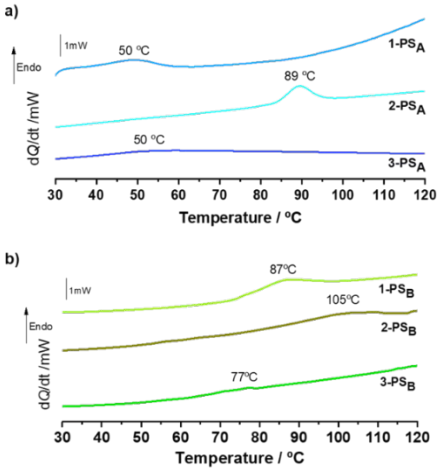

Fig. 6 DSC curves of photosensitive polycarbonates **1–3-PS$_A$** and **1–3-PS$_B$**.

Complementary powder X-ray diffraction analysis revealed typical amorphous patterns for all prepared polymers, with an absence of sharp crystalline diffraction peaks, consistent with their intrinsically non-crystalline nature (Figs. S16 – S21, SI).

Photophysical characterisation

The photosensitive polycarbonates were then analysed by UV-vis spectroscopy to evaluate their photophysical properties and potential photosensitising applications. The UV-vis spectra of the photosensitive polycarbonates, recorded in 2-MeTHF at

room temperature, are presented in Fig. 7 and compared with those of the parent photosensitisers **PS$_A$** and **PS$_B$**. For the Al-phthalocyanine-derived polymers **1–3-PS$_A$**, both absorption and fluorescence emission spectra are shown in the same plot.

The UV-vis spectra of photosensitive polycarbonates **1–3-PS$_A$** exhibited the typical spectral features of monomeric phthalocyanine **PS$_A$**, with a well-resolved and intense sharp Q-band at around ~ 685 nm, a vibronic band near ~ 615 nm and the Soret band in the region of ~ 350-355 nm (Fig. 7a). On the other hand, the UV-vis absorption spectra of the chromium porphyrin-based vinyl-functionalised photosensitive polycarbonate **1-PS$_B$** display the characteristic features of metalloporphyrin **PS$_B$**, including an intense Soret band with absorption maxima at 417 nm and two less intense Q-bands around 560 and 600 nm (Fig. 7b). Differently, the bromo-functionalised photosensitive polycarbonate **3-PS$_B$** shows a red-shifted Soret band at 480 nm, which indicates that, under the employed bromination conditions, bromine substitution may also have occurred at the β-pyrrolic positions of the porphyrin ring.[65]

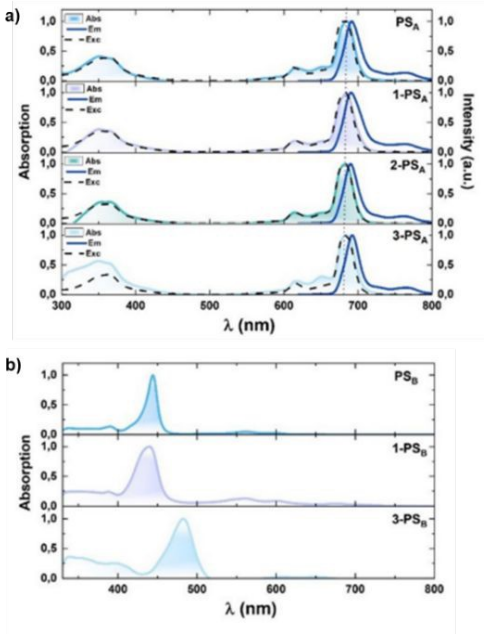

Fig. 7 a) UV-vis absorption and emission spectra obtained for Al(III) phthalocyanine-based functionalized polycarbonates **1–3-PS$_A$**; b) UV-vis absorption spectra obtained for Cr(III) porphyrin-based functionalized polycarbonates **1-PS$_B$** and **3-PS$_B$** (using 2-MeTHF as solvent, at 25 °C).

A summary of photophysical parameters, including wavelength absorption (λ_{abs}), fluorescence emission maxima (λ_{em}), fluorescence quantum yields (φ_F), fluorescence lifetimes (τ_F) and singlet oxygen quantum yields (φ_Δ), is presented in Table 4. The Al(III) phthalocyanine-derived polycarbonates **1–3-PS$_A$** present fluorescence maxima at approximately 690 nm, with the emission spectra being the mirror image of the corresponding absorption ones (Fig. 7a). Small Stokes-shift of 6-8 nm, indicates a similar structure of both the ground and first excited singlet states. In addition, the polycarbonates **1–3PS$_A$** feature fluorescence quantum yields (ϕ_F) between 0.17 and 0.46, while their fluorescence lifetimes were similar (τ_F ~ 6 ns), within the range for reported phthalocyanine compounds.[66] To further estimate the potential of the photosensitive polymers for the photo-inactivation of microorganisms, singlet oxygen sensitisation studies were also performed. It was found that the polycarbonates **1-PS$_A$** and **2-PS$_A$** are capable of generating singlet oxygen at levels comparable to that of the polymer-unbound aluminium phthalocyanine photosensitiser **PS$_A$**. However, the brominated polycarbonate material **3-PS$_A$** exhibited a significantly lower singlet oxygen quantum yield (ϕ_Δ = 0.08). This reduction may be attributed to heavy atom effect, possibly resulting from the partial bromination of the phthalocyanine macrocycle, which is known to promote intersystem crossing to the triplet state, leading to a shorter triplet-state lifetime, thereby reducing the efficiency of energy transfer to molecular oxygen and ultimately limiting singlet oxygen generation.[67] As expected, none of the chromium-based polycarbonate materials exhibited detectable fluorescence emission or singlet oxygen generation under the studied conditions.[68,69]

Table 4 Photophysical data obtained for photosensitive polycarbonates, compared with aluminum phthalocyanine (**PS$_A$**) and chromium porphyrin (**PS$_B$**) photosensitizers

	λ_{abs} (nm)	λ_{em} (nm)	ϕ_F	τ_F	ϕ_Δ
PS$_A$	355/616/685	692	0.17	6.6	0.21
1-PS$_A$	355/615/685	691	0.42	6.1	0.18
2-PS$_A$	355/614/683	690	0.46	6.1	0.19
3-PS$_A$	350/617/684	692	0.28	5.9	0.08
PS$_B$	445/560/600	N.D.	N.D.	N.D.	N.D.
1-PS$_B$	437/560/600	N.D.	N.D.	N.D.	N.D.
3-PS$_B$	480/603/650	N.D.	N.D.	N.D.	N.D.

Measurements were performed using 2-MeTHF as solvent, at 25°C
N.D.: not detectable (below the detection limit). Photophysical data for **2-PS$_B$** was not acquired due to polymer insolubility.

Overall, the photophysical data indicate that polycarbonates functionalisation with different substituents, including vinyl, formyl or dibromoethyl groups, does not induce significant changes in the photophysical parameters of Al phthalocyanine-based polymers **1–3-PS$_A$**. As the singlet oxygen generation efficiency of **1–3-PS$_A$** remained comparable to that of the polymer-unbound Al(III) phthalocyanine (**PS$_A$**), these materials present a strong potential as photosensitive antibacterial systems.

Antibacterial photodynamic inactivation (*a*PDI) studies

Preliminary studies on the antibacterial photodynamic inactivation activity of the Al-phthalocyanine-based polycarbonates **1–3-PS$_A$** were conducted against *Staphylococcus aureus*, a high-priority pathogen associated with antibiotic resistance and hospital-acquired infections.[70,71] The assays were performed using a 96-well plate (Fig. 8), in which polymer-coated wells were exposed to bacterial suspensions and irradiated with red light (660 nm, 49 J cm^{-2}),

View Article Online
DOI: 10.1039/D5PY01211B

followed by colony counting to quantify bacterial survival. The photosensitive polycarbonates **1–3-PS$_A$**, each containing approximately 2% (w/w) of the photosensitiser **PS$_A$**, showed limited photodynamic inactivation against *S. aureus*, achieving only up to a 1-log reduction in colony-forming units (CFU), corresponding to 90% bacterial inactivation. This modest activity is consistent with previous reports on similar low-loaded photosensitizing systems.[72-73] To evaluate whether the low efficacy stemmed from insufficient photosensitiser content, the polymers were further enriched with **PS$_A$** to a final loading of 15% (w/w), as confirmed by UV-Vis spectroscopy, and the **PS$_A$**-enriched materials were re-evaluated under identical light irradiation conditions. Regarding the materials **1-PS$_A$** and **3-PS$_A$** (with 15% **PS$_A$**), a 3-log CFU reduction was observed, indicating bactericidal activity, defined as ≥99.9% inactivation.[74] Remarkably, the formyl-functionalised polymer **2-PS$_A$** (with 15% **PS$_A$**) achieved complete inactivation of the bacterial inoculum (≥7-log CFU reduction), fulfilling the disinfection threshold set by the U.S. Environmental Protection Agency for healthcare settings.[75] Given that all samples contained comparable photosensitiser loadings (~15%), the observed differences in photodynamic inactivation efficiency strongly suggest that the aldehyde functionalities incorporated into the polycarbonate backbone play a synergic role in the photo-antimicrobial activity,[76-80] consistent with our previous findings obtained with porphyrin photosensitisers combined with aldehydes.[72] In contrast, **PS$_B$**-based polymers are not expected to exhibit significant photodynamic activity due to the paramagnetic nature of the chromium(III) centre, which limits efficient generation of reactive oxygen species, and may instead be better suited to alternative applications, such as oxidative catalysis for the degradation of organic pollutants.

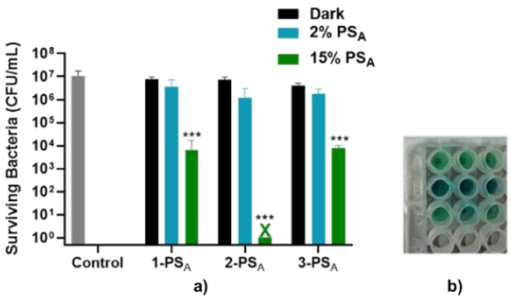

Fig. 8 a) Photodynamic activity of Al(III) phthalocyanine-based photosensitive polycarbonates **1–3-PS$_A$** in inactivation of *S. aureus* planktonic cultures, using 49 J/cm^2 light dose (660 nm LED). The label *** ($p < 0.001$) represents statistical difference relative to the control (light irradiation without photosensitive material); b) Image of the 96-well plate loaded with stock solutions of the photosensitive polycarbonates **1–3-PS$_A$** (83 mg/mL).

Polycarbonate/ethyl cellulose biocomposite films

To investigate the application potential of photosensitive polycarbonates as photo-disinfectant materials, attempts were made to process them into polymer films by solvent casting. However, the resulting films were rigid and brittle, restricting their practical applicability. To overcome this limitation, a polycarbonate-based photosensitive biocomposite film was developed,[81] by blending the polycarbonate with ethyl cellulose, a well-established bio-based plasticiser recognised for its excellent film-forming ability and broad polymer compatibility.[82] Considering the superior efficacy of formyl-functionalised polycarbonate **2-PS$_A$**, enriched with 15% **PS$_A$** (w/w), in the inactivation of *S. aureus* (Fig. 8), the biocomposite formulation was prepared by dissolving **2-PS$_A$** (25 w/w%) and ethyl cellulose (75 w/w%) in cymene, used as a green solvent. After homogenisation, the solution was cast onto a glass plate substrate using a doctor blade applicator to obtain uniform films. The glass plate was then kept in the dark at room temperature to allow solvent evaporation and formation of the biocomposite film **2-PS$_{A(15\%)}$@EC** (Fig. S25, SI). The resulting film (Fig. 9a) was analysed by UV-vis spectroscopy (Fig. 9b), which revealed the characteristic absorption bands of Al-phthalocyanine **PS$_A$** at approximately 614 and 683 nm, confirming that its photophysical properties were retained upon incorporation into the ethyl cellulose composite. The DSC curve of **2-PS$_{A(15\%)}$@EC** (Fig. 9c) shows two glass transitions, one around 70 °C and another near 125 °C. The lower T_g, attributed to the **2-PS$_A$** rich domains, appears at a lower temperature than in pure **2-PS$_A$**. This shift is likely due to interactions with the ethyl cellulose matrix and partial mixing, which might increase the segmental mobility of **2-PS$_A$** chains and reduce their thermal rigidity.[83] The higher T_g corresponds to the ethyl cellulose phase,[84] indicating partial compatibility between the two polymers (polycarbonate and ethyl cellulose) and the formation of a heterogeneous amorphous system.

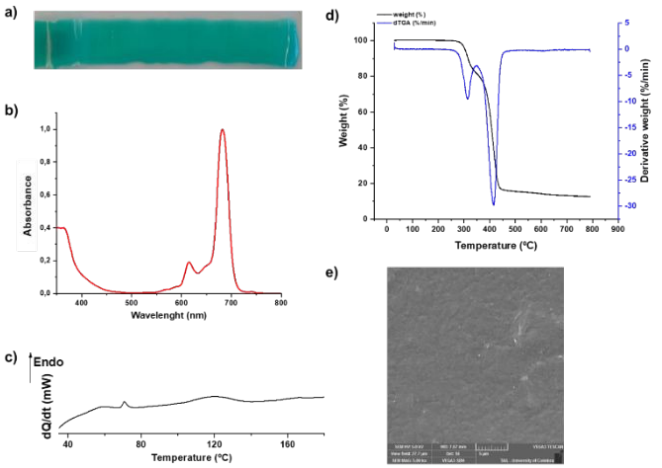

Fig. 9 Characterization of **2-PS$_{A(15\%)}$@EC**: a) image of the biocomposite film; b) UV-Vis spectra, measured in 2-Me-THF at 25 °C; c) DSC/DTG plot; d) TGA curve; e) SEM image (with 5000× magnification).

Complementary TGA analysis of the biocomposite film (Fig. 9d and Table 5) revealed a markedly different degradation profile compared to the **2-PS$_A$** neat polymer. While neat **2-PS$_A$** shows early degradation with a T_{max} around 200 °C (Table 3, entry 2), the composite exhibited T_5 = 304 °C, T_{50} = 407 °C, and T_{max} = 415 °C. These values indicate that the thermal behaviour of the system is dominated by the ethyl cellulose matrix,[85] with no

View Article Online
DOI: 10.1039/D5PY01211B

clear thermal signature from the **2-PS$_A$**. The significant delay of degradation suggests a synergistic effect, where the ethyl cellulose matrix provides a thermally stable environment that suppresses the decomposition of **2-PS$_A$**. The absence of a distinct degradation step for **2-PS$_A$** in the composite profile further supports the strong thermal shielding effect of the matrix. This results in a composite with improved thermal resistance, suitable for applications requiring bio-based materials with high thermal stability. The SEM image (Fig. 9e) showed a rough textured surface with small aggregates dispersed in a smoother background, reflecting the heterogeneous nature of **2-PS$_{A(15\%)}$@EC**.

Table 5 Thermal degradation temperatures of **2-PS$_{A(15\%)}$@EC**

Material	T_5/°C	T_{50}/°C	T_{max}/°C
2-PS$_{A(15\%)}$@EC	304	407	415

T_5 = temperature at 5% weight loss, T_{50} = temperature at 50% weight loss, T_{max} = temperature at maximum degradation rate.

Tensile testing of composite **2-PS$_{A(15\%)}$@EC** revealed markedly improved strength and flexibility. The stress-strain curve (Fig. 10) displays a smooth elastic region, followed by gradual plastic deformation and fracture at a relatively high elongation (42.1%). This response reflects reduced stiffness compared to neat polycarbonate, yielding a film with enhanced ductility and toughness, which are critical attributes for practical applications.

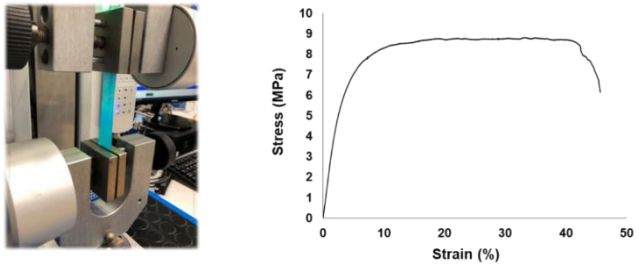

Fig. 10 Tensile (stress-strain) tests of ethyl cellulose-polycarbonate biocomposite **2-PS$_{A(15\%)}$@EC**.

The photo-antimicrobial activity of the biocomposite film **2-PS$_{A(15\%)}$@EC** was also evaluated in *a*PDI assays, by placing film sections in 96-well plates, followed by exposure to *S. aureus* suspensions and irradiation with red light (660 nm, 49 J cm^{-2}). Ethyl cellulose (**EC**) films without **2-PS$_A$** were tested under identical conditions as material control to assess any intrinsic effect of the polymer matrix. Dark controls were performed for both materials by incubating the bacterial suspensions in contact with the films for the same period in the absence of light. Bacterial survival was subsequently quantified by colony counting (Fig. S28, SI). The results revealed the complete inactivation of *S. aureus* in the presence of **2-PS$_{A(15\%)}$@EC** films (≥7-log CFU reduction), confirming the strong photo-antibacterial activity of the material (Fig. 11). As previously observed for polycarbonates **1–3-PS$_A$** (Fig. 8), this effect continues to be exclusively light-dependant, since no antibacterial activity is obtained through just dark incubation. Moreover, this photoinactivation efficacy is only attributable to the presence of **2-PS$_{A(15\%)}$**, as ethyl cellulose without any photosensitizer (**EC**) does not exhibit intrinsic antibacterial activity either in dark or under the applied irradiation conditions (Fig. 11).

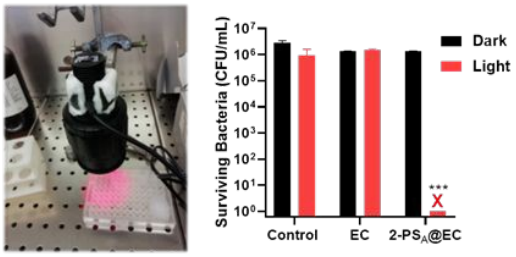

Fig. 11 Photodynamic inactivation of *S. aureus* planktonic cultures with ethyl cellulose-polycarbonate biocomposite **2-PS$_{A(15\%)}$@EC** and ethyl cellulose without **2-PS$_{A(15\%)}$** (**EC**) using either 49 J/cm^2 light dose (660 nm LED) or dark incubation under the same time. The label *** ($p < 0.001$) represents statistical difference relative to the control (light irradiation without photosensitive material).

Therefore, the incorporation of ethyl cellulose not only improved flexibility and processability but also preserved the photodynamic efficacy of the **2-PS$_A$** polycarbonate. These findings highlight the potential of the ethyl cellulose-polycarbonate biocomposite as a photoactive antimicrobial coating for surface disinfection applications.

Experimental

Materials and methods

All reagents and solvents were purchased from commercial suppliers (TCI chemicals, Alfa Aesar, Merck/Sigma Aldrich, Apollo Scientific or STREM chemicals). Solvents were purified and dried according to standard methods. Air and moisture sensitive reagents were manipulated using *Schlenk* techniques, under a nitrogen or argon atmosphere. Glass material was dried in an oven at 150 °C. The tetrapyrrolic macrocycle complexes **PS$_A$** and **PS$_B$** were synthesized accordingly to our previously reported methods and spectroscopic data is in agreement.[33,34] ^{1}H and ^{13}C NMR spectra were recorded in $CDCl_3$ on a Bruker Avance III 400 spectrometer, operating at 400.13 MHz for ^{1}H and 100.61 MHz for ^{13}C. Pseudo-2D ^{1}H NMR DOSY spectra were acquired using the diffusion bipolar pulse pair stimulated echo and LED (LEDBPGP) method, with 32 k complex points, 16 scans per increment, and a spectral width of 4795.34 Hz, at 25 °C. The data were obtained with a diffusion delay of 180 ms and 4 ms small delta, linear gradient pulse amplitudes ranging from 2 to 95% during 2 ms with a total of 64 steps, and an eddy current delay of 5 ms. Temperature calibration was performed using standard samples before each NMR session. Chemical shifts for ^{1}H and ^{13}C are expressed in ppm, relatively to a TMS as internal standard, or relatively to residual peaks, present in the deuterated solvents used, $CDCl_3$ or DMSO-d_6. UV-Visible spectra were obtained on a Shimadzu 2100 spectrophotometer, using glass cells with an optical path of 1 cm. MALDI-TOF mass spectra

were recorded in positive ion mode on a rapifleX MALDI Tissuetyper (Bruker) mass spectrometer using dithranol (DIT) as matrix and sodium trifluoroacetate (NaTFA) as cationisation agent. Samples were dissolved in $CHCl_3$ (50 µL), diluted 1:50 in $CHCl_3$, and mixed with the matrix solution (2 mg DIT in 200 µL MeOH) and NaTFA (1 mg mL^{-1} in THF). An aliquot (1 µL) of the resulting mixture was spotted onto the MALDI plate. Data are reported as mass-to-charge ratios (m/z). Size exclusion chromatography (GPC/SEC) analysis was carried out on a Shimadzu LC-20AD, equipped with index refraction detector RID-20A (Tª 35 ºC), on a column PLgel 5 µm MIXEDC; 2 × (300 × 7.5 mm), from Polymer Laboratories Ltd, using THF as eluent. The polymer sample (3 mg/mL) in THF, was first filtered through a 0.45 µm nylon filter, and then injected (20 µL). Polystyrene standards for calibration (EASYCAL-1 by Polymer Laboratories) were used to determine number average (M_n) and weight-average (M_w) molecular weights, using GPC-Shimadzu software. SEM analyses were carried out in a Zeiss-GEMINI II FESEM operated at an accelerating voltage of 2 kV, using a secondary electron detector. The solid-state infrared spectroscopy studies were carried out using an infrared spectrophotometer with Fourier transform from Thermo Scientific, model Nicolet 380 FT-IR, with an ATR module, model Orbit Diamond from the same brand. The thermogravimetric studies were carried out in a Perkin-Elmer equipment, model STA 6000 connected to a cooling bath (cooling liquid: water-ethylene glycol 1:1, at a temperature of 15 ºC) made by Julabo, model F12. DSC tests were performed using a power compensated differential scanning calorimeter Perkin-Elmer, model DSC7, with a branded circulation bath MGW Lauda as a cooling system (coolant: water-ethylene glycol 1:1, at -20°C). The equipment used to obtain the X-ray diffractograms was a Rigaku powder diffractometer, model MiniFlex 600, connected to a van der Heijden thermostatic bath (water, 20ºC). UV-vis absorption spectra were obtained in a 5 mm or 10 mm quartz cuvette in 2-MeTHF on a Shimadzu UV-2600 spectrophotometer. The emission spectra of the compounds in solution were obtained in fluorescence quartz cuvette of 5 mm or 10 mm path length, using a Horiba-Jobin-Vonn Fluorolog 3.22 spectrometer. All the fluorescence spectra were corrected for the wavelength response of the system. Fluorescence quantum yields for the solution samples were obtained by the absolute method using a Hamamatsu Quantaurus QY absolute photoluminescence quantum yield spectrometer model C11437 (integration sphere). Room-temperature singlet oxygen phosphorescence was detected at 1270 nm with a Horiba-Jobin-Ivon SPEX Fluorog 3.22 using the Hamamatsu R5509-42 photomultiplier previously reported. The use of a Schott RG1000 filter was essential to eliminate from the infrared signal all of the first harmonic contribution of sensitizer emission in the region below 850 m. The singlet oxygen formation quantum yield was then determined by direct measurement of the phosphorescence at 1270 nm following irradiation of the aerated solution of the samples in 2-MeTHF.

Synthetic procedures and characterization

Synthesis of 4-vinylcyclohexane polycarbonate (1-PS_A and 1-PS_B). The tetrapyrrolic macrocycle catalyst **PS_A** or **PS_B** (0.07 mol%) and PPNCl (0.07 mol%) were placed in a glass-lined stainless-steel autoclave, and left in vacuum for approximately 3 h, at 80 °C. Then, 1,2-epoxy-4-vinylcyclohexene (4 ml, 31 mmol), previously dried over alumina, was injected, via cannula, into the autoclave, which was set at the desired temperature (80 °C) and pressurized with of CO_2 (40 bar). The reaction proceeded with stirring (600 rpm) at 80 °C, for 24 h. At the end, the autoclave was cooled and slowly depressurized and the crude was dissolved in CH_2Cl_2, to remove the polymer from the autoclave. After solvent evaporation and drying under vacuum at 100 °C for 12 h, the resulting solid was washed with *n*-hexane (3×) and dried under vacuum at 100 °C for 18 h. The % of conversion was determined by ^{1}H NMR of the crude mixture. Selectivity was calculated by integral ratio between polycarbonate and cyclic carbonate peaks. The CO_2 content (%) was calculated from ^{1}H NMR data by the integral ratio between copolymer carbonate linkages (δ = 4.64 ppm) with respect to the ether linkage signals (δ = 3.57 ppm). Isolated yields (%) were calculated from the mass of the isolated products relative to the weighted mass of epoxide and the CO_2 weight. **1-PS_A** (using **PS_A** as catalyst): Yield 1.981 g (38%). ^{1}H NMR ($CDCl_3$, 400 MHz): δ (ppm) 5.77-5.76 (m, 1H), 5.05-5.02 (m, 2H), 4.90-4.77 (m, 2H) 2.43 (br s, 1H), 1.86-1.57 (br m, 6H). ^{13}C NMR ($CDCl_3$, 100 MHz): δ (ppm) 153.5, 141.7, 113.9, 74.2, 39.2, 35.0, 31.8, 29.5, 26.3. FTIR (ATR, cm^{-1}): 3074, 2925, 2861, 1742, 1640, 1596, 1230. UV-Vis (2-MeTHF, nm): 681, 643, 615. GPC data: M_n = 2943 g/mol, Đ = 1.23. **1-PS_B** (using **PS_B** as catalyst): Yield 4.171 g (80%). ^{1}H NMR ($CDCl_3$, 400 MHz): δ (ppm) 5.79-5.73 (m, 1H), 5.11-4.96 (m, 2H), 4.89-4.77 (m, 2H), 2.43 (br s, 1H), 1.85-1.53 (br m, 6H). ^{13}C NMR ($CDCl_3$, 100 MHz): δ (ppm) 153.5, 141.5, 114.1, 73.5, 35.0, 31.7, 26.2, 25.5. FTIR (ATR, cm^{-1}): 3078, 2940, 2866, 1755, 1643, 1449, 1235, 1080. UV-Vis (2-MeTHF, nm): 602, 560, 438. GPC data: M_n = 11191 g/mol, Đ = 1.41.

Synthesis of 4-(3-oxopropyl)cyclohexane polycarbonate (2-PS_A and 2-PS_B). The vinyl-functionalized polycarbonate **1-PS_A** or **1-PS_B** (840 mg), $Rh(acac)(CO)_2$ (2.58 mg 0.01 mmol) and xantphos (29 mg, 0.05 mmol) were placed in a glass-lined stainless-steel autoclave. Then, toluene (10 mL) was added, via cannula, and the autoclave was purged with three cycles of vacuum and an equimolar mixture of CO/H_2 (*syngas*). The autoclave was set on the desired temperature (80°C), pressurized with *syngas* (20 bar), and the reaction was conducted under these conditions with stirring for 5 h. At the end, the reactor was cooled to room temperature and depressurized. The solvent was evaporated, the resulting solid was washed with *n*-hexane, filtered and dried in vacuum at 80 °C. **2-PS_A**: Yield 871 mg (88%). ^{1}H NMR ($CDCl_3$, 400 MHz) δ (ppm) 9.78 (s, 1H), 4.85-4.78 (m, 2H), 2.49 (br s, 1H), 1.86-1.25 (m, 10H). ^{13}C NMR ($CDCl_3$, 100 MHz): δ (ppm) 202.6, 153.7, 73.5, 41.8, 35.3, 31.2, 30.2, 26.3, 25.7. FTIR (ATR, cm^{-1}): 2935.5, 1818.6, 1722.1, 1433, 1235. UV-Vis (2-MeTHF, nm): 688, 652, 619. GPC data: M_n = 4495 g/mol, Đ = 2.88. **2-PS_B**: Yield

View Article Online
DOI: 10.1039/D5PY01211B

910 mg (92%). FTIR (ATR, cm^{-1}): 2926, 2860, 1819, 1731, 1449, 1225. UV-Vis (solid state, nm): 602, 563, 520, 439.

Synthesis of 4-(1,2-dibromoethyl)cyclohexane polycarbonate (3-PS_A and 3-PS_B). The vinyl-functionalized polycarbonate **1-PS_A** or **1-PS_B** (250 mg) was placed in a round-bottom flask and dissolved in carbon tetrachloride (15 mL). Then, a Br_2 5% solution in carbon tetrachloride (5.7 mL) was added dropwise, at 25 °C, with stirring. After approximately 30 min, the mixture was quenched with an aqueous sodium thiosulfate solution (1 M) and washed brine, and the organic phase was extracted with dichloromethane. Finally, the organic phase was dried with anhydrous sodium sulphate, the solvent was evaporated, and the obtained solid was dried in vacuum at 80 °C. **3-PS_A**: Yield 225 mg (90%). ^{1}H NMR ($CDCl_3$, 400 MHz) δ (ppm) 4.97-4.84 (m, 2H), 4.20 (br s, 1H), 3.85-3.69 (m, 2H), 2.35-2.31 (br s, 1H), 1.99 - 1.63 (m, 7H). ^{13}C NMR ($CDCl_3$, 100 MHz): δ (ppm) 152.6, 75.2, 58.3, 33.0, 29.5, 24.8, 18.4. FTIR (ATR, cm^{-1}): 2930, 2856, 1737, 1430, 1230, 590. UV-Vis (2-MeTHF, nm): 682, 650, 616. GPC data: M_n = 1279 g/mol, Đ = 1.63. **3-PS_B**: Yield 215 mg (86%). FTIR (ATR, cm^{-1}):2939, 2865, 1742, 1434, 1225, 590. UV-Vis (2-MeTHF, nm): 655, 605, 482. GPC: M_n = 10479 g/mol, Đ = 1.40.

Preparation of biocomposite film 2-$PS_{A(15\%)}$@EC. The formyl polycarbonate **2-PS_A** (125 mg) was placed in a round-bottom flask and dissolved in cymene (5 ml), at 25 °C, with stirring. Once fully dissolved, ethyl cellulose (375 mg) was gradually added to the solution. Then, **PS_A** (21 mg) was added and the mixture was stirred continuously for approximately 3 h, in the dark, at 25 °C. Upon observing full homogenization and increased viscosity, the resulting solution was cast onto a glass plate using a doctor blade applicator to obtain uniform films. The coated plates were stored in the dark under ambient conditions and exposed to air for 48 h to allow solvent evaporation and film formation.

Antibacterial photodynamic inactivation (*a*PDI) studies

Photoinactivation assays were carried out using *Staphylococcus aureus* ATCC 29213 as the model microorganism. These bacteria were cultured on Mueller–Hinton (MH) agar for ~24 h at 37 °C on the day prior to testing. A suspension was then prepared in sterile water at a density of 0.5 McFarland standard, corresponding to approximately 1.5×10^8 CFU/mL. Then, in the wells coated with the photosensitive polycarbonate material (or biocomposite film), 20 µL of the bacterial inoculum was added and irradiated with a red LED source (660 ± 20 nm, 20 mW/cm²). The light doses reported were obtained by calculating the total energy emitted by the light source during a given irradiation time, to which a correction factor (0.34) is applied that considers the overlap between the absorption spectrum of **PS_A** and the emission spectrum of the LED (Flg. S26, SI).[86] After irradiation, 80 µL of sterile distilled water was introduced into each well. After homogenization, 10 µL aliquots were collected, serially diluted in sterile water, and plated on MH agar. The plates were incubated at 37 °C for 24 h, after which the surviving bacterial colonies were counted and expressed as CFU/mL, relatively to control experiments, which were performed under identical conditions in the absence of polycarbonate material (Fig. S28, SI). Two distinct methods were followed for preparation of coated wells, depending on the investigated photosensitive material type: polycarbonate powder or ethyl cellulose/polycarbonate biocomposite films.

Photosensitive polycarbonate powders. The polycarbonate material **1–3-PS_A** (125 mg) was dissolved in acetone (1.5 mL). Then, aliquots of 40 µL (83 mg/mL) were transferred into the wells of a 96-well polypropylene round-bottom plate, and the solvent was allowed to evaporate at room temperature, forming a uniform thin film at the bottom of each well.

Photosensitive ethyl cellulose/polycarbonate biocomposite film. Circular sections (6 mm diameter, 0.7 mm thickness) of the ethyl cellulose-based photosensitive biocomposite film **2-$PS_{A(15\%)}$@EC** (5 mg) were cut and placed in the wells of a 96-well polypropylene round-bottom plate.

Conclusions

We have described a sustainable and versatile strategy for the synthesis of multifunctional CO_2-based photosensitive polycarbonates. The one-pot CO_2/epoxide copolymerisation, using tetrapyrrolic macrocyclic metal complexes (aluminium phthalocyanine or chromium porphyrin) as dual-function catalysts and integrated photosensitisers, afforded polycarbonates with high carbonate content (95-99%) and enabled efficient incorporation of chromophore units directly into the polymer backbone, avoiding post-grafting steps thereby reinforcing the process sustainability. The presence of pendant vinyl groups along the polymer chains provided a robust and modular platform for post-polymerisation functionalisation, significantly expanding the chemical versatility of these CO_2-based materials. Rh-catalysed hydroformylation afforded aldehyde-functionalised polycarbonates with excellent chemo- and regioselectivity, representing the first example of this transformation applied to CO_2-derived polycarbonates, while bromination offered an alternative route for fine-tuning polymer structure and functionality. Detailed structural, spectroscopic and thermal characterisation confirmed preservation of the intrinsic photophysical properties of the tetrapyrrolic macrocycles, together with the robustness and tunability of the materials. Notably, the Al-phthalocyanine-based polycarbonates exhibited high fluorescence quantum yields (ϕ_F up to 0.46) and efficient singlet oxygen generation (ϕ_Δ up to 0.21), highlighting their suitability for light-driven applications. To address the intrinsic brittleness of the neat polycarbonates and progress towards processable materials, an ethyl cellulose-based biocomposite film was successfully developed. The resulting biocomposite preserved the key photophysical characteristics of the photosensitive polycarbonate while exhibiting enhanced flexibility, thermal stability and film-forming ability, demonstrating an effective translation of molecular-level design into macroscopic functional materials. Preliminary

View Article Online
DOI: 10.1039/D5PY01211B

antibacterial photodynamic inactivation studies illustrated the potential of the aluminium phthalocyanine-based polycarbonate materials for light-triggered antimicrobial applications, serving as a proof of concept for future surface and coating technologies. Overall, this study expands polymer chemistry by integrating CO_2 valorisation, post-polymerisation modification and biocomposite processing, establishing a sustainable synthetic platform for next-generation photosensitive materials with tunable properties and broad application prospects.

Author contributions

A.C.S. Gonzalez: Investigation, data curation, writing – review and editing; R. T. Aroso: Investigation, data curation, formal analysis; C. Cunha: Investigation, data curation; J. S. S. Melo: Formal analysis, validation; M. E. S. Eusébio: Formal analysis, validation; T. M. R. Maria: Formal analysis, validation; G. J. da Silva: Validation; R. M. M. Brito and P. F Cruz: NMR data collection and NMR DOSY acquisition, Formal analysis; R. M. B. Carrilho and M. M. Pereira: Conceptualisation, methodology, formal analysis, supervision, validation, funding acquisition, writing – original draft, writing – review and editing.

Conflicts of interest

The authors do not have any conflicts to declare.

Data availability

The data supporting this article, including NMR spectra, GPC-SEC chromatograms, X-ray diffraction have been included as part of the Electronic Supplementary Information (ESI) available. See DOI:

Acknowledgements

The authors acknowledge the Coimbra Chemistry Centre – Institute of Molecular Sciences (CQC-IMS) which is funded by the Fundação para a Ciência e a Tecnologia (FCT), through project UIDB/00313/2025 (DOI: https://doi.org/10.54499/UID/00313/2025) and by the European Union - *NextGenerationEU* through PRR UID/PRR/00313/2025 (DOI: https://doi.org/10.54499/UID/PRR/00313/2025) and UID/PRR2/00313/2025 d https://doi.org/10.54499/UID/PRR2/00313/2025). The Institute of Molecular Sciences is funded by FCT through project LA/P/0056/2020 (DOI: https://doi.org/10.54499/LA/P/0056/2020). We also thank UC/Santander for funding through Project CO2PhotoBioPlas (Provas de Conceito 2023 - PT0051.B.04.E) and Project nº 6979 - PRODUTECH R3 [Recuperação-Resiliência-Reindustrialização, financed by PRR - Recovery and Resilience Plan and by the European Union Next Generation EU Funds. NMR data was collected at the UC-NMR facility (https://uc.pt/uc-nmr/) supported in part by grants from FCT, FEDER and PRR. A.C.S.G. thanks FCT for the PhD grant UI/BD/150804/2020.

References

1 O. Bertrand and J.-F. Gohy, Photo-responsive polymers: synthesis and applications, *Polym. Chem.*, **2017**, *8*, 52–73.
2 F. Xu and B. L. Feringa, Photoresponsive Supramolecular Polymers: From Light-Controlled Small Molecules to Smart Materials, *Adv. Mater.*, 2023, **35**, 2204413.
3 T. Zubair, M. M. Hasan, R. S. Ramos and R. M. Pankow, Conjugated polymers with near-infrared (NIR) optical absorption: structural design considerations and applications in organic electronics, *J. Mater. Chem. C*, 2024, **12**, 8188–8216.
4 M. A. Nagar and D. Janner, Polymer-Based Optical Guided-Wave Biomedical Sensing: From Principles to Applications, *Photonics*, 2024, **11**, 972.
5 D. Zhao, X. Li, Q. Li, C. Yue, Y. Wang and H. Li, Self-healing photoluminescent polymers with photosensitive behavior for information storage and multiple-level dynamic encryption, *Chem. Sci.*, 2024, **15**, 13306–13312.
6 S. Sun, C. Yuan, Z. Xie, W.-C. Xu, Q. Zhang and S. Wu, Photoresponsive nanostructures of azobenzene-containing block copolymers at solid surfaces, *Polym. Chem.*, 2022, **13**, 411–419.
7 S. Inacker, P. Kahler and N. Hampp, Enhancing the photochemical reversibility of coumarin-containing polymers by molecular orientation control, *Polym. Chem.*, 2022, **13**, 6238–6245.
8 K. Takada, Synthesis of biobased functional materials using photoactive cinnamate derivatives, *Polym. J.*, 2023, **55**, 1023–1033.
9 V. Pruthi, Y. Akae and P. Théato, Photoresponsive Spiropyran and DEGMA-Based Copolymers with Photo-Switchable Glass Transition Temperatures, *Macromol. Rapid Commun.*, 2023, **44**, 2300270.
10 M. R. Hamblin, Antimicrobial photodynamic inactivation: a bright new technique to kill resistant microbes, *Curr. Opin. Microbiol.*, 2016, **33**, 67–73.
11 T. Maisch, Photoantimicrobials - an update, *Transl. Biophotonics*, 2020, **2**, e201900033.
12 S. Gnanasekar, G. Kasi, X. He, K. Zhang, L. Xu and E.-T. Kang, Recent advances in engineered polymeric materials for efficient photodynamic inactivation of bacterial pathogens, *Bioact. Mater.*, 2023, **21**, 157–174.
13 M. P. Wylie, N. J. Irwin, D. Howard, K. Heydon and C. P. McCoy, Hot-melt extrusion of photodynamic antimicrobial polymers for prevention of microbial contamination, *J. Photochem. Photobiol. B: Biol.*, 2021, **214**, 112098.
14 C. P. McCoy, E. J. O'Neil, J. F. Cowley, L. Carson, Á. T. De Baróid, G. T. Gdowski, S. P. Gorman and D. S. Jones, Photodynamic antimicrobial polymers for infection control, *PLoS One*, 2014, **9**(9), e108500.
15 F. Mao-Chun, H. Tomoya and U. Mitsuru, Recent progress in thermally stable and photosensitive polymers, *Polym. J.*, 2018, **50**, 57–76.
16 P. Han-Wen, Y. Kai, S. Yizhi, C. Dan, S. Zhao-Yan, G. Tao, L. Dandan and S. Ke, Photopolymerization activated by photobase generators and applications: from photolithography to high-quality photoresists, *Polym. Chem.*, 2024, **4**, 248–268.

17 M. Jiang, J. Wu, W. Liu, H. Ren, W. Zhang, C.-S. Lee and P. Wang, Self-assembly of Amphiphilic Porphyrins To Construct Nanoparticles for Highly Efficient Photodynamic Therapy, *Chem. Eur. J.*, 2021, **27**, 11195–11204.

18 P. Zhang, C. Xu, X. Zhou, R. Qi, L. Liu, F. T. Lv, Z. Li and S. Wang, Cationic conjugated polymers for enhancing beneficial bacteria adhesion and biofilm formation in gut microbiota, *Colloids Surf. B: Biointerfaces*, 2020, **188**, 110815.

19 J. Chen, X. Tao, L. Tao, H. Li, C. Li, X. Wang, C. Li, R. Li and Q. Yang, Novel conjugated organic polymers as candidates for visible-light-driven photocatalytic hydrogen production, *Appl. Catal. B: Environmental*, 2019, **241**, 461–470.

20 A. Bahar, S. Belhabib, S. Guessasma, F. Benmahiddine, A. E. A. Hamami and R. Belarbi, Novel conjugated organic polymers as candidates for visible-light-driven photocatalytic hydrogen production, *Energies*, 2022, **15**, 3686.

21 J. P. Jayachandran, H. A. Reed, H. Zhen, L. F. Rhodes, C. L. Henderson, S. A. B. Allena nd P. A. Kohl, Air-channel fabrication for microelectromechanical systems via sacrificial photosensitive polycarbonates, *J. Microelectromech. Syst.*, 2003, **12**, 147–159.

22 W. Yu, E. Maynard, V. Chiaradia, M. C. Arno and A. P. Dove, Aliphatic Polycarbonates from Cyclic Carbonate Monomers and Their Application as Biomaterials, *Chem. Rev.*, 2021, **121**, 10865–10907.

23 Z. Skafi, L. A. Castriotta, B. Taheri, F. Matteocci, M. Fahland, F. Jafarzadeh, E. Joseph, A. Chakraborty, V. Singh, V. Mottaghitalab, L. Mivehi, F. Brunetti, L. Sorbello, A. Di Carlo and T. M. Brown, Flexible Perovskite Solar Cells on Polycarbonate Film Substrates, *Adv. Energy Mater.*, 2024, **14**, 2400912–2400924.

24 T. Taniguchi, N. Shirota, T. Okazoe, S.-I. Matsuoka, K. Yamamotoa and M. Suzuki, Fluorine-driven amorphous solid-state polycondensation: phosgene-free synthesis of high-molecular weight polycarbonate from fluorinated carbonate, *Polym. Chem.*, 2024, **15**, 508–515.

25 A. Tsuda, N. Ozawa, R. Muranaka, T. Kuwahara, A. Matsune and F. Liang, Photo-on-Demand *In Situ* Phosgenation Reactions That Cross Three Phases of a Heterogeneous Solution of Chloroform and Aqueous NaOH, *ACS Omega*, 2023, **8**, 27802–27810.

26 M. Kawamoto, Y. Mori, A. Tsuge and T. Endo, Anionic ring-opening polymerization behavior of trans-cyclohexene carbonate using metal tert-butoxides: Construction of living anionic ring-opening polymerization by lithium *tert*-butoxide, *J. Polym. Sci.*, 2022, **60**, 1416–1421.

27 H. Phan, K. Kortsen, G. Englezou, B. Couturaud, A. J. Nedoma, A. K. Pearce and V. Taresco, Functional initiators for the ring-opening polymerization of polyesters and polycarbonates: An overview, *J. Polym. Sci.*, 2020, **58**, 1911–1923.

28 M. Benaglia, A. Alberti, L. Giorgini, F. Magnoni and S. Tozzi, Poly(glycidyl methacrylate): a highly versatile polymeric building block for post-polymerization modifications, *Polym. Chem.*, 2013, **4**, 124–132.

29 M. Rimmele, F. Glocklhofer and M. Heeney, Post-polymerisation approaches for the rapid modification of conjugated polymer properties, *Mater. Horiz.*, 2022, **9**, 2678–2697.

30 Q. Huang, W.-Z. Wang, S. Liu, X.-G. Jia, L. Xia, F.-L. Qin, Q. Wang, Y. Liu and H.-J. Li, Green fabrication of carbon dioxide-based polycarbonates with durable antimicrobial properties and UV resistance, *Chem. Eng. J.*, 2023, **477**, 147107.

31 P. Holzmüller, J. Preis and H. Frey, CO_2-based polycarbonates from biobased cyclic terpenes with end-of-life usage potential, *Polym. Chem.*, 2024, **15**, 3657–3666.

32 E. V. Chernikova and I. P. Beletskaya, From epoxides and carbon dioxide to polycarbonates: synthesis, properties and applications, *Russ. Chem. Rev.*, 2024, **93**, RCR5112.

33 R. M. B. Carrilho, L. D. Dias, R. Rivas, M. M. Pereira, C. Claver and A. M. Masdeu-Bultó, Solventless Coupling of Epoxides and CO_2 in Compressed Medium Catalysed by Fluorinated Metalloporphyrins, *Catalysts*, 2017, **7**, 210.

34 A. C. S. Gonzalez, A. P. Felgueiras, R. T. Aroso, R. M. B. Carrilho and M. M. Pereira, Al(III) phthalocyanine catalysts for CO_2 addition to epoxides: Fine-tunable selectivity for cyclic carbonates versus polycarbonates, *J. Organomet. Chem.*, 2021, **950**, 121979.

35 I. Kim, M. J. Yi, S. H. Byun, D. W. Park, B. U. Kim and C. S. Ha, Biodegradable Polycarbonate Synthesis by Copolymerization of Carbon Dioxide with Epoxides Using a Heterogeneous Zinc Complex, *Macromol. Symp.*, 2005, **224**, 181–192.

36 M. Taherimehr, J. P. C. C. Sertã, A. W. Kleij, C. J. Whiteoak and P. P. Pescarmona, New Iron Pyridylamino-Bis(Phenolate) Catalyst for Converting CO_2 into Cyclic Carbonates and Cross-Linked Polycarbonates, *ChemSusChem*, 2015, **8**, 1034–1042.

37 P.-M. Lin, C.-H. Chang, H.-J. Chuang, C.-T. Liu, B.-T. Ko and C.-C. Lin, Bimetallic Nickel Complexes that Bear Diamine-Bis(Benzotriazole Phenolate) Derivatives as Efficient Catalysts for the Copolymerization of Carbon Dioxide with Epoxides, *ChemCatChem*, 2016, **8**, 984–991.

38 L.-S. Huang, C.-Y. Tsai, H.-J. Chuang and B.-T. Ko, Copolymerization of Carbon Dioxide with Epoxides Catalyzed by Structurally Well-Characterized Dinickel Bis(benzotriazole iminophenolate) Complexes: Influence of Carboxylate Ligands on the Catalytic Performance, *Inorg. Chem.*, 2017, **56**, 6141–6151.

39 H.Y. Zhang, B.Y. Liu, H.N. Ding, J.W. Chen and Z.Y. Duan, Polycarbonates derived from propylene oxide, CO_2, and 4-vinyl cyclohexene oxides terpolymerization catalyzed by bifunctional salcyCoIIINO3 complex and its post-polymerization modification, *Polymer*, 2017, **129**, 5–11.

40 C.-H. Chang, C.-Y. Tsai, W.-J. Lin, Y.-C. Su, H.-J. Chuang, W.-L. Liu, C.-T. Chen, C.-K. Chen and B. T. Ko, Alternating copolymerization of epoxides with carbon dioxide or cyclic anhydrides using bimetallic nickel and cobalt catalysts: Preparation of hydrophilic nanofibers from functionalized polyesters, *Polymer*, 2018, **141**, 1–11.

41 Y.-C. Su, C.-Y. Tsai, L. S. Huang, C.-H. Lin and B.-T. Ko, Synthesis and characterization of di-nuclear bis(benzotriazole iminophenolate) cobalt complexes: catalysis for the copolymerization of carbon dioxide with epoxides, *Dalton Trans.*, 2019, **48**, 12239–12249.

42 Y.-C. Su, C.-T. Chen and B.-T. Ko, Catalysis and kinetics for alternating copolymerization of carbon dioxide with epoxides using dinuclear nickel catalysts of pyrazolyl based diamine-bisphenolate ligands, *Polymer*, 2020, **200**, 122553.

43 Y.-C. Su and B. -T. Ko, Alternating Copolymerization of Carbon Dioxide with Epoxides Using Highly Active Dinuclear Nickel Complexes: Catalysis and Kinetics, *Inorg. Chem.*, 2021, **60**, 852–865.

44 Y. Chen, W.C. Wang, D. Xie, L. Wu and C.C. Zhang, Synthesis of CO_2-based functional poly(carbonate-co-lactide), *J. Polym. Sci.*, 2021, **59**, 1528–1539.

45 G. -L. Liu and B. -T. Ko, Alternating copolymerization of carbon dioxide with alicyclic epoxides using bimetallic nickel(II) complex catalysts containing benzotriazole-based salen-type derivatives: Catalysis and kinetics, *Polymer*, 2022, **260**, 125371.

46 H. -F. Hsu, G. -L. Liu, Y.-C. Su and B. -T. Ko, Bimetallic nickel complexes containing imidazole-based phenolate ligands as

efficient catalysts for the copolymerization of carbon dioxide with epoxides, *Dalton Trans.*, 2024, **53**, 299–314.

47 G.-L. Liu, Y.-C. Su, W.-H. Chuang and B.-T. Ko, Synthesis and Characterization of Heterodinuclear Indium(III)/Sodium(I) Complexes Containing Benzotriazole-Derived Phenolate Ligands: Effective Catalysts for Ring-Opening Copolymerization of Carbon Dioxide with Epoxides, *Inorg. Chem.*, 2024, **63**, 19582–19592.

48 Z.-Y. Liu, G.-L. Liu and B.-T. Ko, Catalytic copolymerization of epoxides with phthalic anhydride or carbon dioxide by effective binuclear zinc and nickel complexes: Catalysis and kinetics, *Eur. Polym. J.*, 2025, **222**, 113619.

49 C. G. Fan, Q. Y. Ge, S. J. Lu, X. S. Feng, Y. F. Tu, L. Jia, S. H. Lin, Q. M. Pan and F. T. T. Ng, One-Pot Synthesis of Polycarbonate-*b*-Polyester Block Copolymers From CO_2/Epoxide/ε-Caprolactone Catalyzed by Salen-Cobalt(III) Complex, *J. Polym. Sci.*, 2025, **63**, 1217–1225.

50 D. J. Darensbourg, W.-C. Chung, C. J. Arp, F.-T. Tsai and S. J. Kyran, Copolymerization and Cycloaddition Products Derived from Coupling Reactions of 1,2-Epoxy-4-cyclohexene and Carbon Dioxide. Postpolymerization Functionalization via Thiol–Ene Click Reactions, *Macromolecules* 2014, **47**, 7347–7353.

51 M. Hassan, G. A. Bhat and D. J. Darensbourg, Post-polymerization functionalization of aliphatic polycarbonates using click chemistry, *Polym. Chem.*, **2024**, *15*, 1803–1820.

52 Z. Xie, X. Wang, Z. Chen and H. Jiang, Palmitoylated cellulose nanocrystal/polycarbonate composite with high mechanical performance and good transparency, *J. Appl. Polym. Sci.*, 2023, **140**, e53298.

53 Y. Zhang, X. Wang, Y. Li and J. Li, Cellulose nanocrystals composites with excellent thermal stability and high tensile strength for preparing flexible resistance strain sensors, *Carbohydr. Polym. Technol. Appl.*, 2022, **3**, 100214.

54 P. C. J. Kamer, P. W. N. M. van Leeuwen and J. N. H. Reek, Wide Bite Angle Diphosphines: Xantphos Ligands in Transition Metal Complexes and Catalysis, *Acc. Chem. Res.*, 2001, **34**, 895–904.

55 Z. Freixa and P. W. N. M. van Leeuwen, Bite angle effects in diphosphine metal catalysts: steric or electronic?, *Dalton Trans.*, 2003, **10**, 1890–1901.

56 F. M. S. Rodrigues, L. D. Dias, M. J. F. Calvete, T. M. R. Maria, L. M. Rossi, A. J. L. Pombeiro, L. M. D. R. S. Martins and M. M. Pereira, Immobilization of Rh(I)-N-Xantphos and Fe(II)-C-Scorpionate onto Magnetic Nanoparticles: Reusable Catalytic System for Sequential Hydroformylation/Acetalization, *Catalysts,* 2021, **11**, 608.

57 Y. Yoshida, A. Nishiyama and S. Inoue, Synthesis and Reactions of Polycarbonate with Pendant Vinyl Groups, *Polym. J.*, 1982, **14**, 327–330.

58 Y.-L. Kuan, C.-W. Chu, W.-T. Du and S.-W. Kuo, Design Chemical Structures of CO_2-Derived Poly(cyclohexene carbonate) Copolymers to Mediate Intra-/Intermolecular Interactions with Strong Hydrogen-Bonded Donor Homopolymer, *Macromolecules*, 2025, **58**, 1090–1102.

59 T.-J. Hsu and C.-S. Tan, Block copolymerization of carbon dioxide with cyclohexene oxide and 4-vinyl-1-cyclohexene-1,2-epoxide in based poly(propylene carbonate) by yttrium–metal coordination catalyst, *Polymer*, 2002, **43**, 4535–4543.

60 D. T. Carrillo, A. D. Diaz, Nonlinear Response of a Polycarbonate in Post-Yield Cyclic Tests, *Polymers*, 2025, **17**, 1535.

61 S. Zhang, B. Wang, X. Meng and Y. Chen, Nonlinear Response of a Polycarbonate in Post-Yield Cyclic Tests, *Materials*, 2023, **16**, 3386.

62 M. Gelmont, M. Yuzefovitch, D. Yoffe, E. Eden and S. Levchik, Alkylation of Aromatic Compounds with Pentabromobenzyl Bromide and Tetrabromoxylene Dibromide as a New Route to High Molecular Weight Brominated Flame Retardants, *Polymers*, 2020, **12**, 352.

63 C. Li, Q. Ran, R. Zhu and Y. Gu, Study on thermal degradation mechanism of a cured aldehyde-functional benzoxazine, *RSC Adv.*, 2015, **5**, 22593–22600.

64 I. C. McNeill and M. Ćoşkun, Structure and stability of halogenated polymers: Part 4—Chain brominated polystyrene, *Polym. Degrad. Stab.*, 1989, **25**, 1–9.

65 S. Rayati, S. Zakavi, S. H. Motagh, V. Noroozi, M. Razmjoo, A. Wojtczak and A. Kozakiewicz, β-Tetra-brominated meso-tetraphenylporphyrin: A conformational study and application to the Mn-porphyrin catalyzed epoxidation of olefins with tetrabutylammonium oxone, *Polyhedron*, 2008, **27**, 2285–2290.

66 Z. Neduvhuledza, T. Nkaki, M. Louzada, T. Nyokong and S. Khene, Photophysical and nonlinear optical properties of the positional isomers of 4-(4-tertbutylphenoxy) substituted cobalt, nickel and copper phthalocyanines, *Opt. Mater.*, 2020, **109**, 110195.

67 R. Bonnett and G. Martínez, Photobleaching of Sensitisers Used in Photodynamic Therapy, *Tetrahedron*, 2001, **57**, 9513–9547.

68 N. Sinha, P. Herr, L. González and O. S. Wenger, A Near-Infrared-II Emissive Chromium(III) Complex, *Angew. Chem. Int. Ed.*, 2021, **60**, 23722–23728.

69 R. E. McClean and L. Pasternack, Kinetics of the reactions vanadium ($a^4F_{3/2}$, $a^6D_{3/2}$) + OX (X = O, N and CO), *J. Phys. Chem.*, **1992**, *96*, 9828–9831.

70 World Health Organization, *Bacterial Priority Pathogens List: Bacterial Pathogens of Public Health Importance to Guide Research, Development and Strategies to Prevent and Control Antimicrobial Resistance*, Geneva, WHO **2024**.

71 R. T. Aroso, F. A. Schaberle, L. G. Arnaut and M. M. Pereira, Photodynamic disinfection and its role in controlling infectious diseases, *Photochem. Photobiol. Sci.*, 2021, **20**, 1497–1545.

72 M. F. C. Silva, R. T. Aroso, J. M. Dabrowski, B. Pucelik, A. Barzowska, G. J. da Silva, L. G. Arnaut and M. M. Pereira, Photodynamic inactivation of E. coli with cationic imidazolyl-porphyrin photosensitizers and their synergic combination with antimicrobial cinnamaldehyde, *Photochem. Photobiol. Sci.*, 2024, **23**, 1129–1142.

73 F. M. S. Rodrigues, I. Tavares, R. T. Aroso, L. D. Dias, C. V. Domingos, C. M. G. de Faria, G. Piccirillo, T. M. R. Maria, R. M. B. Carrilho, V. S. Bagnato, M. J. F. Calvete and M. M. Pereira, Photoantibacterial Poly(vinyl)chloride Films Applying Curcumin Derivatives as Bio-Based Plasticizers and Photosensitizers, *Molecules,* 2023, **28**, 2209.

74 Clinical and Laboratory Standards Institute, *Methods for Determining Bactericidal Activity of Antimicrobial Agents; Approved Guideline M26-A*, Wayne, PA, USA, CLSI **1999**.

75 U.S. Environmental Protection Agency, *Product Performance Test Guidelines: Disinfectants for Use on Environmental Surfaces – Guidance for Efficacy Testing; OCSPP 810.2200*, Washington, DC, **2018**. Available at: https://www.regulations.gov/document?D=epa-hq-oppt-2009-0150-0036

76 J. Zhang, Z. Chen, D. Zeng, Y. Xia, Y. Fan, X. Zhang, N. Li, X. Liu, X. Sun, S. Zhao, J. Zhang, J. Liu and Q. Sun, Antibacterial and rapidly absorbable hemostatic sponge by aldehyde modification of natural polysaccharide, *Commun. Mater.*, 2024, **5**, 129.

View Article Online
DOI: 10.1039/D5PY01211B

77 H. Deng, W. Zhang, Y. Ramezan, Z. Riahi, A. Khan and Z. Huang, Antibacterial and antioxidant plant-derived aldehydes: A new role as cross-linking agents in biopolymer-based food packaging films, *Compr. Rev. Food Sci. Food Saf.*, 2025, **24**, e70089.

78 D. N. Amato, D. V. Amato, Y. Adewunmi, O. V. Mavrodi, K. H. Parsons, S. N. Swilley, D. A. Braasch, W. D. Walker, D. V. Mavrodi and D. L. Patton, Using Aldehyde Synergism to Direct the Design of Degradable Pro-Antimicrobial Networks, *ACS Appl. Bio Mater.*, 2018, **1**, 1983–1991.

79 G. Bisignano, M. G. Laganà, D. Trombetta, S. Arena, A. Nostro, N. Uccella, G. Mazzanti and A. Saija, In vitro antibacterial activity of some aliphatic aldehydes from Olea europaea L., *FEMS Microbiol. Lett.*, 2001, **198**, 9–13.

80 Y. Zi, M. Zhu, X. Li, Y. Xu, H. Wei, D. Li and C. Mu, Effects of carboxyl and aldehyde groups on the antibacterial activity of oxidized amylose, *Carbohydr. Polym.*, 2018, **192**, 118–125.

81 R. M. B. Carrilho, M. M. Pereira, A. C. S. Gonzalez, R. T. P. M. Aroso, G. Piccirillo and F. M. S. Rodrigues, WIPO (PCT), WO2025014383A2, 2025.

82 T.-Y. Yu, Y.-K. Tseng, T.-H. Lin, T.-C. Wang, Y.-H. Tseng, Y.-H. Chang, M.-C. Wu and W.-F. Su, Effect of cellulose compositions and fabrication methods on mechanical properties of polyurethane-cellulose composites, *Carbohydr Polym.*, 2022, **291**, 119549.

83 K. Olonisakin, A. K. Mohanty, M. Thimmanagari and M. Misra, Recent advances in biodegradable polymer blends and their biocomposites: a comprehensive review, *Green Chem.*, 2025, **27**, 11656–11704.

84 H.L. Lai, K. Pitt and D. Q. M. Craig, Characterisation of the thermal properties of ethylcellulose using differential scanning and quasi-isothermal calorimetric approaches, *Int. J. Pharm*., 2010, **386**, 178–184.

85 M. K. Trivedi and A. Branton, Characterization of Physicochemical and Thermal Properties of Biofield Treated Ethyl Cellulose and Methyl Cellulose, *Int. J. Biomed. Mater. Res.*, 2015, **3**, 83–91.

86 F. A. Schaberle, Assessment of the actual light dose in photodynamic therapy, *Photodiagnosis Photodyn. Ther.*, 2018, **23**, 75–77.

View Article Online
DOI: 10.1039/D5PY01211B

Data availability

The data supporting this article, including NMR spectra, GPC-SEC chromatograms, X-ray diffraction have been included as part of the Electronic Supplementary Information (ESI) available. See DOI: